THE ROLE OF SECONDARY ALUMINOSILICATE MINERALS IN TECHNETIUM-99 IMMOBILIZATION IN RADIOACTIVE WASTE

By

JOHNBULL OTAH DICKSON

A dissertation submitted in partial fulfillment of
the requirements for the degree of

DOCTOR OF PHILOSOPHY

WASHINGTON STATE UNIVERSITY
Department of Crop and Soil Sciences

AUGUST 2014

ProQuest LLC.
789 East Eisenhower Parkway
P.O. Box 1346
Ann Arbor, MI 48106 - 1346

To the Faculty of Washington State University:

The members of the Committee appointed to examine the dissertation of

JOHNBULL OTAH DICKSON find it satisfactory and recommend that it be accepted.

_____

James B. Harsh, Ph.D., Chair

_____

Markus Flury, Ph.D.

_____

Eric M. Pierce, Ph.D.

Acknowledgements

Many people have played pivotal roles in helping me complete this dissertation. First and foremost, I want to express my deepest gratitude to Dr. James Harsh for his guidance and mentoring throughout my postdoctoral study. His useful advice, constructive comments and insightful suggestions have helped to improve the overall quality of this dissertation. On an interpersonal level, he is easily approachable and one of the nicest people I have had the opportunity to work with. His cool demeanor, truly caring nature has made the arduous task of going through graduate studies more manageable and fulfilling. I also thank Dr. Harsh for believing in me and for all the financial support throughout my studies.

I'm deeply grateful to Dr. Markus Flury for his kindness, guidance and superb mentoring. He was very instrumental in helping with manuscripts review/editing for publications. His astute teaching style is second to none and has further inspired me to pursue an academic career. I remain indebted to Dr. Eric Pierce for his friendship and mentoring. He provided guidance for my experimental designs and financial support for my research. He was very instrumental in connecting me with other scientists for assistance with data analysis.

I would like to acknowledge the following individuals for their countless help: Jeffrey Boyle for his tireless help with XRD, IC, AAS measurements and friendship and support; The Department of Crops and Soil sciences; Rick Conrey and Charles Knaack, WSU GeoAnalytical Laboratory, for XRF and ICP-MS measurements.

I thank Drs. Christine Davitt and Valerie Lynch-Holm for the training on the SEM and TEM instruments at the WSU Franceschi Microscopy and Imaging Center. Special

thanks to the members of my soil chemistry/physic group for their friendships and constructive critiques of my work: Mike Grant, Melissa Letourneau, Zhenqing Shi, Waled S Omar Suleiman, Thorsten Knappenberger, Jessica Mullane, Hamid Iqbal, Nirmalya Chatterjee, Ziru (Steven) Liu and Surachet Aramrak.

I am grateful to the following organizations for providing funding for this work: the U.S. Department of Energy (DOE), Office of Science, Biological and Environmental Research Program (SBER), under contract No. DE-PS02-09ER65075; Mineralogical Society of American, and the Bullitt Foundation.

Finally, I would like to express my sincere gratitude to my parents, Mr. Okundaye and Mrs. Patience Okundaye, my beloved siblings: Eunice, Kehinde, Taiye, Iyore, Iyobo and Rowland. Also special thanks to Mrs. Irina Bobkova, for her motherly love and endless support.

THE ROLE OF SECONDARY ALUMINOSILICATE MINERALS IN TECHNETIUM-99 IMMOBILIZATION IN RADIOACTIVE WASTE

Abstract

by Johnbull Otah Dickson, Ph.D.

Washington State University

August 2014

Chair: James Harsh

Corroding waste tanks at select U.S. Department of Energy's nuclear waste facility have leaked highly alkaline tank waste solutions containing radionuclides and other contaminants into subsurface sediments. These tank wastes react with subsurface sediments to form secondary mineral phase(s) (feldspathoids), which may play key role in the transport of contaminants through the vadose zone and aquifers. Although transformation of secondary precipitates in subsurface sediments has been extensively studied, there is lack of knowledge about the role of feldspathoid selectivity in controlling the long-term fate and transport of key anionic radionuclides in the subsurface. The overarching objectives of this dissertation were to (1) determine secondary mineral transformation with aging time, alkalinity, anion type and selectivity, and (2) quantify the competitive incorporation of ReO_4^- (a chemical analogue for Tc-99) into mineral phase(s) as a function of anion composition, size and selectivity. The key results of this work showed that alkalinity, time and anion composition play important role in mineral

transformations that control the mobility of key radionuclide species in the environment. Nitrite and chloride anions predominantly promote sodalite phase(s) formation. Nitrate in 16 mol OH^-/kg solution favored cancrinite nucleation while in 1 mol OH^-/kg solution fostered mixed cancrinite/sodalite formation. The sequestering capacity of sodalite for ReO_4^- was ~5 times higher than that of cancrinite. The immobilized ReO_4^- in the sodalite cages was not easily exchanged with other competing anions. Due to the less distortion to the β-cage, sodalite displayed stronger preference for smaller competing anions relative to the larger ReO_4^- anion. The selectivity of the mixed sodalite cage for ReO_4^- was largely driven by the difference in anion radii (DIR) and increases in the following order: $Cl^-<NO_3^-<MnO_4^-$ and $CO_3^{2-}<SO_4^{2-}<WO_4^{2-}$ for the monovalent and divalent anions respectively. When the DIR between ReO_4^- and competing anions was less than ~12%, then ReO_4^- incorporation into sodalite was significant. The results imply that anion size is the major factor that determines sodalite anion compositions and that ReO_4^- is likely to serve as a suitable analogue for TcO_4^-

Table of Contents

Acknowledgements ..... **iii**

Abstract ..... **v**

Dedication ..... **xii**

Introduction **1**

1.1 Background 1

1.2 Scope and Objectives 5

1.3 Dissertation Outline and Attributions 6

Competitive Incorporation of Perrhenate **8**

and Nitrate into Sodalite **8**

2.1 Abstract 8

2.2 Introduction 10

2.3 Experimental Methods 12

2.3.1 Hydrothermal Synthesis 12

2.3.2 Characterization 13

2.4 Results and Discussion 15

2.4.1 Structure of Mixed Sodalite 15

2.4.2 Composition Analysis 16

2.4.3 Rhenium Valence in Mixed Sodalite 17

2.4.4 Morphology of Synthesis Product 17

2.4.5 Reaction Time Experiment 18

2.4.6 Effect of Aging Time 18

2.4.7 Effect of Anion Types 19

2.4.8 Competitive Incorporation of NO_3^- and ReO_4^- into Mixed Sodalite 20

2.5 Tables and Figures 24

Appendix **33**

Supporting Information **33**

A.1 X-ray Absorption Near Edge Structure (XANES) Spectroscopy 33

Perrhenate Incorporation into Binary Mixed Sodalites: 38

The Role of Anion Size and Implications for 38

Technetium-99 Sequestration 38

3.1 Abstract 38

3.2 Introduction 40

3.3 Materials and Methods 42

3.3.1 Rhenium as Analogue for Tc 42

3.3.2 Hydrothermal Mineral Synthesis 42

3.3.3 Powder X-ray Diffraction 43

3.3.4 X-ray Absorption Near Edge Structure (XANES) Spectroscopy 44

3.3.5 Electron Microscopy 44

3.3.6 Chemical Analysis 45

3.4 Results 45

3.4.1 Synthesis Product Morphology 45

3.4.2 Composition Analysis 46

3.4.3 Mineral Structure 46

3.4.4 Rhenium Oxidation State 47

3.5 Discussion 47

3.5.1 Incorporation of ReO_4^- in the Presence of Competing Anion (X) 47

3.6 Environmental Implications for ^{99}Tc Immobilization. 49

3.7 Tables and Figures 52

Immobilization and Exchange of Perrhenate in 63

Sodalite and Cancrinite 63

4.1 Abstract 63

4.2 Introduction 65

4.3 Experimental Methods 67

4.3.1 Mineral Synthesis 67

4.3.2 Perrhenate exchange with NO_2^- and NO_3^- 68

4.4 Characterization of solid phases 68

4.4.1 Powder X-ray Diffraction Identification 68

4.4.2 Electron Microscopy 69
4.5 Results 69
4.5.1 Structures 69
4.5.2 Morphology 70
4.5.3 Rhenium Uptake 71
4.5.4 Desorption Experiment 71
4.6 Discussion 72
4.6.1 Effect of Alkalinity 72
4.6.2 Feldspathoid Formation in the Presence of Different Anions 73
4.6.3 Feldspathoid Formation with Time 73
4.6.4 Effect of ReO_4^- concentration on feldspathoid formation 74
4.6.5 Stability of ReO_4^- to Ion Exchange 75
4.6.6 Anion Template Effects on Feldspathoid Formation 75
4.7 Conclusions and Implications 76
4.8 Tables and Figures 78

Summary and Conclusions 88

Bibliography 91

Lists of Tables

Table 2.1: Conditions for hydrothermal syntheses 25
Table 2.2: Refined powder X-ray data for mixed-anion sodalite 26
Table 2.3: Chemical composition data for pure and mixed sodalite 27
Table A.1: Result of XANES spectra fitting for ReO_4/NO_3-sodalite 34
Table 3.1: Particle size data for mixed-anion sodalites. 53
Table 3.2: Mixed anion sodalite chemical composition data 54
Table 3.3: Refined powder X-ray data for mixed-anion sodalite. 55
Table 3.4: XANES spectral fitting results for mixed-anion sodalites. 55
Table 3.5: Ionic radii, hydration energy and ionic potential data for studied anions 56
Table 4.1: Summarized conditions for the hydrothermal syntheses. 79
Table 4.2: Unit cell and refinement parameters for mixed-anion feldspathoid 79
Table 4.3: Particle size data for select mixed-anion feldspathoid. 80
Table 4.4: Feldspathoid weight fraction and ReO_4^-/anion concentrations. 80
Table 4.5: Solution ReO_4^- after aqueous exchange with NO_2^- or NO_3^- 80

Lists of Figures

Figure 1.1: Hanford site location and principle facilities 2
Figure 2.1: Face-sharing truncated octahedra of ReO_4-sodalite framework 28
Figure 2.2: Refined powder X-ray spectra for selected mixed-anion sodalite 29
Figure 2.3: X-ray absorption spectral data for ReO_4/NO_3-sodalite. 30
Figure 2.4: SEM micrographs of Re/NO_3-sodalites. 31
Figure 2.5: Selectivity graph for rhenium incorporation into ReO_4/NO_3 sodalite 32
Figure A.1: SEM micrographs of 0.003 – 0.006 Re/NO_3-sodalites.....35
Figure A.2: Variation of ReO_4^- concentration in mixed sodalites with aging time 36
Figure A.3: Dependence of the unit cell parameter on ReO_4^- 37
Figure 3.1: SEM images of mixed-anion sodalite 57
Figure 3.2: EDS spectra for mixed-anion sodalites 58
Figure 3.3: Refined powder X-ray spectra for mixed-anion sodalites. 59
Figure 3.4: Rhenium L_2-XANES spectral data for ReO_4/MnO_4-sodalite 60
Figure 3.5: The dependence of lattice parameter on $r_{AB} = [r_A(M_A) + (M_{1-A})r_B]$. 61
Figure 3.6: The distribution coefficient (K_d) graph for ReO_4^- in mixed-anion sodalite 62
Figure 4:1: Refined powder X-ray spectra for mixed-anion feldspathoids.....81
Figure 4.2: SEM images of ReO_4/X-feldspathoids. 82
Figure 4.3: TEM images of mixed-anion feldspathoids 83
Figure 4.4: Mixed-anion feldspathoid particles size. 84
Figure 4.5: ReO_4^- incorporated into mixed-anion feldspathoids.....85
Figure 4.6: Variation of ReO_4^- in feldspathoids with ReO_4^-/X^- solution ratios. 86
Figure 4.7: The dependence of lattice parameter on $r_{AB} = [r_A(M_A) + (M_{1-A})r_B]$ graph. 87

Dedication

This dissertation is dedicated to my deceased parents – Mr. Dickson Okundaye, and Mrs. Patience Okundaye for your unconditional love, support and encouragement. You continue to inspire me to be a better person in this journey called life.

You are greatly missed.

Chapter 1

Introduction

1.1 Background

From 1943 to 1989, large amounts of high-level radioactive wastes (HLW) were generated at the U.S. Department of Energy's (DOE) Hanford site as a result of chemically processing of (bismuth phosphate, redox and, uranium and plutonium recovery by extraction) spent fuels for nuclear weapon production. The 586-square mile Hanford site is located on the Columbia Plateau (Basin) in southeastern Washington State (Figure 1.1). The Columbia River borders the Hanford site, flowing in a north-northeasterly direction through the site (Gee et al., 2007). The high-level radioactive wastes containing an approximately 1900 kg of technetium-99 (^{99}Tc) were stored underground in 149 single-shell steel-lined concrete tanks and 28 double-shell tanks that hold an estimated volume of 246 million liters (Gephart and Lundgren, 1998). Additionally technetium-99 was also disposed of at the Hanford site via cribs and trenches, which received in excess of 189 million liters of reprocessed tank waste. Seventy-seven single-shell tanks were reported to have leaked high-level radioactive wastes into the vadose zone (Gephart and Lundgren, 1998).

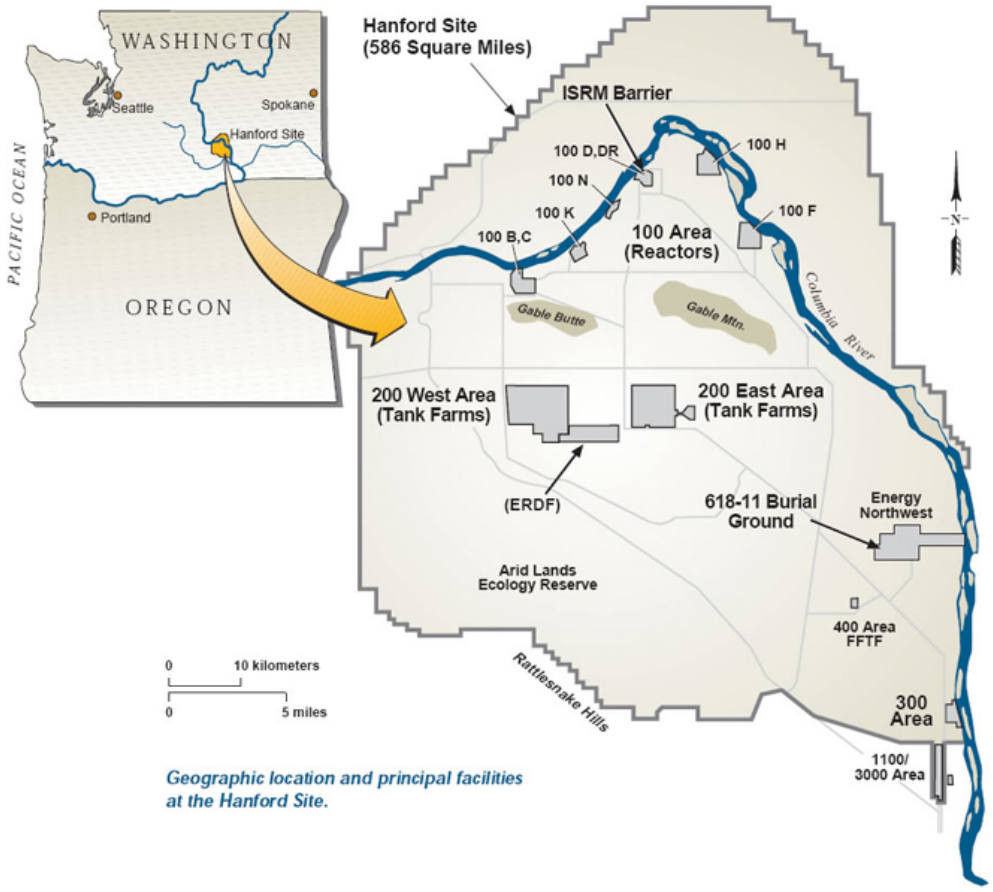

Geographic location and principal facilities at the Hanford Site.

Figure 1.1: Hanford site location and principle facilities. Image is from http://www.hanford.gov/images.cfm/Hanford.map large.jpg (accessed July 10, 2014)

The waste composition is highly variable from tank to tank and is characterized as a highly alkaline (pH is 10 to >14; concentration of free OH^- is ~2 M, while Na^+ ion is ≤19.6 M), high in ionic strength (I = 2 – 14 M), and close to saturation with an $Al(OH)_3$ phase(s) (Lichtner and Felmy, 2003; Mashal et al., 2004). The waste contains numerous byproducts from the ^{239}Pu recovery and waste treatment processes including Na^+, $Al(OH)_4^-$, OH^-, NO_3^-, NO_2^-, CO_3^{2-}, Cl^-, SO_4^{2-}, PO_4^{3-} and Ni^+, and aluminum and iron oxyhydroxide sludges (Kaplan and Serne, 1998; Qafoku et al., 2003b). Furthermore the HLW contains several contaminants of concern, including CrO_4^{2-}, $^{137}Cs^+$, $^{90}Sr^{2+}$, TcO_4^-, $^{79}SeO_4^{2-}$, and NO_3^-. Because the Hanford site soil and sediment in the vadose zone are predominantly negatively charged key anionic radionuclides (^{125}I, ^{99}Tc and ^{75}Se) are sorbed weakly to the subsurface sediments, leading to their unimpeded migration into the vadose zone water and groundwater (Zachara et al., 2007). This raises concerns over the fate and mobility of leaking waste stream in the vadose zone. Given the estimated inventory of ^{99}Tc in the waste, a long half-life of 211,000 years and the high mobility as TcO_4^- under aerobic conditions, ^{99}Tc migration into the vadose zone water and groundwater poses long-term environmental risk hazard.

Geochemical transport modeling predicted the leaching of ^{99}Tc inventory (5.31×10^3 Ci) into the groundwater table at concentrations in excess of the maximum allowable contaminant level of 0.4 nmol L^{-1} (USDOE., 1997). Surprisingly, nearly 50 years after the release of Tc-99, data from borehole soil/sediment samples collected at varying depths within the Hanford site indicate that a significant portion of ^{99}Tc is associated with an recalcitrant (acid-soluble) phase(s) that is relatively immobile in the deep vadose zone (Serne et al., 2010). Thus, it appears that the Hanford deep vadose zone functions

as a natural barrier for ^{99}Tc contained in the migrating waste stream. This raises the critical question of whether the transformation of native Hanford sediment into secondary precipitates (feldspathoids) is sequestering ^{99}Tc in the subsurface sediment.

Previous investigations have demonstrated that radionuclides, metals, and anions can be incorporated into the feldspathoids (e.g., sodalite, cancrinite) that formed when tank leachate reacts with native Hanford sediments at elevated temperature and hyper-alkalinity (Chorover et al., 2008; Deng et al., 2006a; Deng et al., 2006b). Mattigod et al. (2002; 2006) indicated that rhenium (Re), a nonradioactive surrogate for Tc-99, can be incorporated as ReO_4^- into sodalite minerals by substituting for Cl^-or SO_4^{2-} in the mineral frameworks (Mattigod et al., 2006; Mattigod et al., 2002). The transformation of secondary precipitates in Hanford site sediments has been the subject of many studies (Deng et al., 2006a; Mashal et al., 2004; Qafoku et al., 2004).

Therefore, the knowledge of porous framework materials (feldspathoids) selectivity for competing anion species in a waste streams are critical in determining their efficacy as sequestering phases for waste management and development of remediation strategies. This study will help clarify the role of feldspathoids in the long-term fate and transport of ^{99}Tc below the leaking Hanford tanks. Furthermore it will provide key insights into the preferred anions, and the dependence of preference on size for different sodalite compositions. Additionally it will help shed light on the extent and how anions are incorporated into the sodalite, formed in subsurface and engineered wastes, vitrification processes and chemical weathering by-products.

1.2 Scope and Objectives

The general goal of this work is to better understand the competitive incorporation of ReO_4^- (a close chemical analogue for $^{99}TcO_4^-$) in the presence of smaller competing anions into sodalite formed in highly alkaline conditions of Hanford tank waste solutions and engineered waste forms, with special emphasis on anion retention and selectivity. Feldspathoid, zeolite and other neoformed mineral phases are likely to form under such alkaline conditions, but the exact products will be dependent upon the stability and kinetics of the neoformed minerals (precipitates). The fate and transport of radionuclides and contaminants of concern released from the leaking waste tanks and other waste forms will be impacted by the neoformed mineral phases. The hypothesis of this study is that feldspathoids will have higher affinity for the smaller competing anion X (Cl^-, CO_3^{2-}, NO_3^-, SO_4^{2-}) over ReO_4^-, and the large difference in anion size will lead to nonlinear selectivity with respect to Re/anion composition of feldspathoids.

The main objectives are:

1. To quantify the extent of ReO_4^- incorporation into mixed perrhenate/nitrate sodalite as a function of anion composition and selectivity;
2. To determine the effect of competing anions (X) ranging in size and charge: Cl^-, CO_3^{2-}, SO_4^{2-}, MnO_4^-, and WO_4^{2-} on ReO_4^- incorporation into mixed-anion sodalite; and
3. To determine the role of solution composition (Cl^-, NO_2^-, and NO_3^-), alkalinity and, aging time on formation of sodalite and cancrinite in the presence of ReO_4^- and the exchangeability of ReO_4^- from feldspathoids.

1.3 Dissertation Outline and Attributions

This dissertation consists of five chapters.

1. Chapter 1 (Introduction) provides a brief introduction to the dissertation studies, background information, and overall objectives.
2. Chapter 2 was submitted as a journal article to Environmental Science and Technology: Dickson, J. O.; Harsh, J.B.; Flury, M.; Lukens, W.W.; Pierce, E.M. (2014), Competitive incorporation of perrhenate and nitrate into sodalite.

   This chapter discuses the competitive incorporation of perrhenate (ReO_4^-), a $^{99}TcO_4^-$ chemical analogue, into sodalite in the presence of nitrate (NO_3^-). We examined the formation of sodalite in the presence of NO_3^- and ReO_4^- anions in solutions mimicking Hanford tank leaks. The perrhenate/nitrate sodalites were characterized by bulk chemical analysis, X-ray diffraction, scanning electron microscopy and X-ray absorption near edge structure spectroscopy (XANES). The paper was structured and written, for the most part, by me with assistance regarding editing and suggestions from all the coauthors. Theoretical and experimental ideas and designs were jointly developed by Dr. Harsh and myself. Drs. Flury and Pierce provided further editing and helpful suggestions.
3. Chapter 3 was submitted as a journal article to Chemical Geology: Dickson, J. O.; Harsh, J.B.; Lukens, W.W.; Pierce, E.M. (2014), Perrhenate incorporation into binary mixed sodalites: The role of anion size and Implications for technetium-99 sequestration.

   The chapter highlights the effect of anion of different size and charge on perrhenate incorporation into mixed-anion sodalite. Using a batch experiments

the mixed sodalites were synthesized and anion selectivity was studied as a function of size and charge. The paper was structured and mostly written by me with considerable editorial support and guidance from Dr. Harsh. Theoretical and experimental ideas and designs were jointly developed by Dr. Harsh and myself. Drs. Flury, Pierce and Lukens provided further editing and suggestions.

4. Chapter 4 was prepared to be submitted as a journal article to Applied Geochemistry, J. O.; Harsh, J.B.; Flury, M.; Pierce, E.M. (2014), Immobilization and exchange of perrhenate in sodalite and cancrinite.

   The chapter reviews the effects of competing anions (X) such as OH^-, Cl^-, NO_2^-, and NO_3^- on feldspathoid formation and, ReO_4^- incorporation and exchangeability from feldspathoids. The paper was structured and written, for the most part by me with numerous editing, suggestions and, content revisions by Dr. Harsh. Dr. Harsh and myself jointly developed the theoretical and experimental ideas and designs. Drs. Flury and Pierce provided additional editorial assistance and advice.

5. Chapter 5 presents an overall summary and conclusion from this study.

Chapter 2

Competitive Incorporation of Perrhenate and Nitrate into Sodalite

2.1 Abstract

Nuclear waste storage tanks at the Hanford site in southeastern Washington have released highly alkaline solutions, containing radioactive and other contaminants, into subsurface sediments. When this waste reacts with subsurface sediments feldspathoid minerals (sodalite, cancrinite) are formed, which can sequester pertechnetate ($^{99}TcO_4^-$) into their structure, thereby affecting the fate and transport of TcO_4^- in the vadose zone. This study investigates the potential for incorporation of perrhenate (ReO_4^-), a chemical surrogate for $^{99}TcO_4^-$, into mixed perrhenate/nitrate (ReO_4^-/NO_3^-) sodalite. Mixed-anion sodalites were hydrothermally synthesized in the laboratory from zeolite A in sodium hydroxide, nitrate, and perrhenate solutions at 90°C for 24 to 168 hours. The resulting solids were characterized by bulk chemical analysis, X-ray diffraction, scanning electron microscopy and X-ray absorption near edge structure spectroscopy (XANES) to determine the products' chemical composition, structure, morphology, and Re oxidation state. XANES data indicate that rhenium (Re) was incorporated as $Re(VII)O_4^-$.

This chapter has been submitted to a technical journal: Dickson, J.O., Harsh, J.B., Flury, M., Lukens, W.W., Pierce, E.M. (2014), Competitive incorporation of perrhenate and nitrate into sodalite. *Environ. Sci. Technol.* (submitted)

The non-linear increase of the unit cell parameter with increasing ReO_4^-/NO_3^- ratios suggests formation of two separate sodalite phases in lieu of a mixed-anion sodalite. The results reveal that the sodalite cage is highly selective towards the NO_3^- over ReO_4^-, suggesting that incorporation of NO_3^- into the cage is energetically more favorable than incorporation of the larger ReO_4^-. Based on these results, it is expected that NO_3^-, which is present at significantly higher concentrations in alkaline waste solutions than $^{99}TcO_4^-$, will be strongly preferred for incorporation into the sodalite cage.

2.2 Introduction

Technetium-99 presents a major environmental concern due to its long half-life (211,000 y) and high mobility of pertechnetate, TcO_4^-, in oxidized subsurface systems (Agnew et al., 1997). At the U.S. Department of Energy's Hanford site, approximately 1900 kg of ^{99}Tc was generated and stored underground in 177 tanks, which contain an estimated volume of 65 million gallons of nuclear waste from the production of plutonium during the Cold War era (Gephart and Lundgren, 1995). Seventy-seven of these tanks have leaked high-level radioactive wastes (HLW) into the vadose zone, which extends 50 to 70 meters below the storage tanks (Gephart and Lundgren, 1995). In addition ^{99}Tc was also released to the subsurface via cribs and trenches, which received in excess of 50 million gallons of reprocessed tank waste. Due to weak adsorption of TcO_4^- to the predominantly negatively-charged, oxic sediments prevalent at the Hanford site, ^{99}Tc migration into the vadose zone water and groundwater is expected to be largely unimpeded (Zachara et al., 2007).

The Hanford tank waste solutions are alkaline (pH is 10 to >14; concentration of free OH^- is ~2 M, while Na^+ ion is ≤19.6 M), high in ionic strength (I = 2 – 14 M), and close to saturation with an $Al(OH)_3$ phase (Golcar et al., 2000; Lichtner and Felmy, 2003; Mashal et al., 2004). The tanks contain several contaminants of concern, including CrO_4^{2-}, $^{137}Cs^+$, $^{90}Sr^{2+}$, TcO_4^-, $^{79}SeO_4^{2-}$, and NO_3^-, which have been detected in groundwater. Model simulations of ^{99}Tc transport in the vadose zone suggests that the groundwater concentrations beneath the cribs and trenches in the central plateau should be in excess of the maximum allowable contaminant level of 0.4 nmol/L (USDOE., 1997). Interestingly, nearly 50 years after being released, ^{99}Tc data from

borehole soil/sediment samples collected at varying depths within the central plateau of the Hanford site indicate that a significant portion of ^{99}Tc is present in a relatively immobile form (Serne et al., 2010). One potential explanation that has been proposed by previous studies is the reduction of TcO_4^- to immobile TcO_2 (Tc^{4+}) by iron-bearing minerals present in the vadose zone (Pearce et al., 2014; Peretyazhko et al., 2012). An alternative explanation for the observed ^{99}Tc behavior may be attributed to $^{99}TcO_4^-$ intercalation into feldspathoid phases.

Previous laboratory studies have shown that when simulated tank leachate reacts with native Hanford sediments, the primary and secondary (alumino) silicate minerals dissolve to form precipitates such as allophane, zeolite, and feldspathoids (e.g., sodalite, cancrinite) (Chorover et al., 2008; Qafoku et al., 2004). These investigations demonstrated that sodalite minerals—$[Na_8(Al_6Si_6O_{24})(NO_3)_2]$—incorporate ^{90}Sr and ^{137}Cs from HLW, by replacing Na in the structure (Choi et al., 2006; Deng et al., 2006a). Recent work by Pierce et al. (2014, submitted) has shown that a ReO_4^-/TcO_4^- mixed sodalite with demonstrated TcO_4^- retention can be synthesized in the laboratory.

Feldspathoid minerals have a three-dimensional, oxygen-tetrahedral framework containing Al and Si in a network system with multiple channels, cages and pores (Depmeier, 2005; Frising and Leflaive, 2008). A typical feldspathoid is represented by the general formula $M_8(Al_6Si_6O_{24})X_2$, where M is a metal cation—e.g. Cs, K, Na,—and X is an anion—such as Br^-, Cl^-, I^-, TcO_4^-, ReO_4^-, or SO_4^{2-} (Depmeier, 2005). Sodalite consists of alternating TO_4 corner-sharing tetrahedra (where T is usually Si or Al) forming four and six ring cages, which make up the so-called β- or a sodalite cage (Figure 2.1). These cages are ~6.5 Å in diameter and are accessible through the 2.6 Å-

wide six-membered rings that form continuous channels for diffusion of intra-framework ions (Barrer and Vaughan, 1971; Fazal, 2011; Missimer and Rutherford, 2013). The six-membered ring is occupied by four cations tetrahedrally associated with an anion (e.g., Cl^-) at the center of the cage. With the exception of hydroxide, anions are irreversibly trapped within the cages and once cages are formed it become difficult to replace anions without destroying the cage (Acar et al., 2003).

The role of feldspathoids in attenuating the migration of anionic forms of radionuclides such as TcO_4^- and I^- remains an open and critical question. The incorporation of TcO_4^- into sodalite may play an important role in waste containment below the Hanford waste tanks. Therefore, using Re as a ^{99}Tc surrogate, (1) we examine the formation of sodalite in the presence of NO_3^- and ReO_4^- anions, (2) the preferred oxyanion selectivity, and (3) the possibility of a linear relationship between ReO_4^-/NO_3^- concentration in the solid and anion/cage size. The objective is to quantify the extent of ReO_4^- incorporation into mixed perrhenate/nitrate sodalite as a function of anion composition. Results of this study will clarify the role of feldspathoids in the long-term fate and transport of ^{99}Tc below Hanford tanks, and, ultimately, will help manage waste containment.

2.3 Experimental Methods

2.3.1 Hydrothermal Synthesis

The ReO_4^-/NO_3^- sodalites were hydrothermally synthesized from zeolite 4A using the following modification of a method described by Liu and Navrotsky (2007):

Mixed sodalites were synthesized in a 60-mL Teflon® digestion bombs, filled with 20 mL of de-ionized water, 1 g of NaOH pellets and 0.5 g of zeolite 4A. While keeping the

total molarity constant (1.77 *M*), different molar ratios of $NaNO_3$ and $NaReO_4$ (0.25 to 9.0 NO_3^-/ ReO_4^-) were added to the basic solutions. All chemical reagents were used as received. The bombs were capped, agitated and heated at 90°C in an oven for 24 to 168 hours. The supernatant solutions were decanted and the solid precipitates washed three times with deionized water (0.054×10^{-3} dS/m) by centrifugation at 17,000 rcf. The white solids were dried at 70^0C for 24 hours, weighed and dialyzed against deionized water until the electrolytic conductivity was ≤0.01 dS/m. Typical dialyzed solid yield was 0.5 – 0.6 g. The conditions for the hydrothermal synthesis are summarized in Table 2.1.

2.3.2 Characterization

2.3.2.1 Powder X-ray Diffraction

X-ray diffraction (XRD) patterns were used for phase identification, morphological composition (phase purity), and structural analysis. Samples were hand crushed in mortar and pestle, evenly smeared on zero-background Si holders and characterized by one of the following instruments: (1) Panalytical Xpert diffractometer (XRD) scanning at 0.02° steps and at a rate of 1.5°/min over 5 – 90° 2θ using MoKα radiation (λ = 0.709319 Å). The diffractometer used an X'Celerator detector equipped with either ¼° fixed divergence slits and/or ½° anti-scatter slit. (2) Siemens diffractometer (D500 XRD) scanning at 0.05° steps over 5 – 90° 2θ using Ni-filtered CuKα radiation (λ = 1.54050 Å) and a graphite monochromator equipped with a scintillator detector.

Both X-ray diffractometers used radiation generated at 35 - 40 keV and 30 – 40 mA and a 5 – 10 s dwell time at each step. A mineral search match was conducted using “Jade” and/or HighScore software and the ICDD database. Rietveld refinements of crystallographic data of powder samples were performed by using GSAS with EXPGUI

interface and/or HighScore software packages (Toby, 2001) by varying the detector background, unit cell, Na position, N/Re occupancy, peak shape (U, V, W, and two other peak shapes), overall thermal parameter (B), and preferred orientation. These phases—$[Na_8(AlSiO_4)_6(NO_2)_2]$, $[Na_8(AlSiO_4)_6(ReO_4)_2]$, and $[Na_6Ca_{1.5}(AlSiO_4)_6(CO_3)_{1.5}(H_2O)_{1.75}]$ (Buhl and Lons, 1996; Hackbarth et al., 1999; Mattigod et al., 2006)—were used as reference structures for the refinement.

2.3.2.2 X-ray Absorption Near Edge Structure (XANES) Spectroscopy

Sodalite samples, consisting of powdered sodalite mixed with boron nitride were mounted on an aluminum holder with Kapton windows. XANES measurements were performed at the Stanford Synchrotron Radiation Lightsource (SSRL) at the 11-2 beamline by using the Si (220) double crystal monochromator (f = 90 crystals), detuned 50% to reduce the harmonic content of the beam. XANES spectra were collected from 0.2 keV below to 10 keV above the Re L_2-edge (11.959 keV). Data were either collected in transmission mode using nitrogen-filled ion chambers or fluorescence mode using a 100-element Ge detector and were corrected for detector dead time. Data were reduced from raw data to spectra using SixPack and normalized using Artemis (Ravel and Newville, 2005). Normalized XANES spectra were fit using standard spectra in the locally written program 'fites', which utilizes a non-linear least squares fitting data. Two reference spectra, ReO_2, and pure ReO_4-sodalite, were used for data fitting. The sample XANES spectra were allowed to vary in energy during fitting and the spectral resolution is 7 eV based on the width of the white line at the Re L_2-edge.

2.3.2.3 Electron Microscopy

Scanning electron micrographs were obtained by sputter-coating powder samples with platinum-palladium to 2-nm thickness. Powder samples were subsequently examined under a scanning electron microscope (FESEM) equipped with a field emission gun (FEI Quanta 200F, FEI Co., Hillsboro, OR) and Everhart-Thornley detector. The FESEM has an accelerating voltage of 30 keV with a resolution of 1 nm.

2.3.2.4 Chemical Digestion

Dialyzed powder samples were digested in 3% nitric acid and analyzed for Na concentration by atomic emission and/or absorption spectrophotometry (Varian 220 Flame Atomic Absorption Spectrometer, Varian Ltd., Mulgrave, Australia) and for Si and Al colorimetrically by the silicomolybdous acid method and 8-hydroxyquinoline-butyl acetate method respectively (Bloom et al., 1978; Weaver et al., 1968). Chemical composition of the solid for Re was analyzed by inductively coupled plasma-mass spectrometer (Agilent 7700 ICP-MS). Concentration of NO_3^- was determined by flow injection analysis using the QuikChem 8000 series (Lachat Instruments, Inc., Milwaukee, WI).

2.4 Results and Discussion

2.4.1 Structure of Mixed Sodalite

The refined XRD scans of the pure and mixed anion sodalites are displayed in Figure 2.2. Based on the refinement data, a small amount of cancrinite (~10 weight % on average) is formed along with the pure and mixed sodalite. For the mixed sodalites,

predominance of well-defined X-ray diffraction peaks consistent with the $P\bar{4}3n$ space group and other minor peaks belonging to cancrinite ($P6_3$ space group) were observed.

Cancrinite is characterized by a systematic absence of X-ray diffraction for 0,0,*l* reflections where *l* = odd, while sodalite lacks systematic diffraction peaks for *h,k,l* reflections where *h+k+l* = odd (Buhl and Lons, 1996; Grundy and Hassan, 1982). The main distinguishing diffraction peaks for cancrinite correspond to the (101) and (211) Miller indices with d-spacings of ≈4.67 Å and 3.24 Å, respectively. These characteristic *d*-spacings are absent for sodalite diffraction pattern. The X-ray powder diffraction pattern for the sodalite phases indicate either a pure or a mixed-anion phase(s). Lattice and refinement parameters for both the pure and mixed sodalites are shown in Table 2.2. Based on the Rietveld refinements, the space group $P\bar{4}3n$ and lattice parameters: *a* = 8.9762 Å, 9.1532 Å were adopted for the pure NO_3 and ReO_4-sodalites respectively. The space group $P6_3$ and the calculated lattice parameters: *a* = 12.683 Å and *c* = 5.1827 Å were assigned to the minor phase NO_3-cancrinite, which are in good agreement with previously reported literature values (Buhl et al., 2000; Liu et al., 2005). For the ReO_4/NO_3-sodalites, the refined cell parameters ranged from 8.9808 to 8.9987 Å and an exponential dependence with increasing weight fractions of ReO_4^- in the mixed sodalite lattice occurred.

2.4.2 Composition Analysis

The chemical composition of the synthesis products is shown in Table 2.3. The rationales for assignments of all elements to the sodalite formula are based on the fact that only sodalite and a small amount of cancrinite were detected by XRD. Sodalite and cancrinite have related chemical structures: instead of β-cages, cancrinite contains non-

intersecting channels with the same diameter (Barrer and Vaughan, 1971). The XRD peaks for cancrinite are consistent with a pure NO_3-cancrinite phase(s). The pure ReO_4 and NO_3-sodalite phases contained 1.94 and 1.99 mol of ReO_4^- and NO_3^-, respectively, per formula unit. The mixed sodalite contained from 0.01 – 0.14 mol of ReO_4^-, much lower than its concentration relative to NO_3^- in solution and one order of magnitude lower than expected for no selectivity for ReO_4^- versus NO_3^-. The data demonstrate significant preference for the smaller NO_3^- (1.96 Å) relative to ReO_4^- (2.60 Å).

2.4.3 Rhenium Valence in Mixed Sodalite

The XANES data for select mixed sodalites were fit using only the spectra of $ReO_{2(s)}$ and perrhenate sodalite. The fit results are presented in Table A.1 (Supporting Information 1), and the spectra of the sample along with the reference spectra used in the fitting are displayed in Figure 2.3. In all cases, the spectrum of ReO_4-sodalite contributes significantly to the fit with insignificant contribution from the spectrum of ReO_2. The upper limit of Re(IV) in the sodalite samples is twice the standard deviation – 12%. These data confirm that the mixed sodalite incorporated Re mostly as $Re(VII)O_4^-$.

2.4.4 Morphology of Synthesis Product

The morphology of the powder samples formed in the presence of either ReO_4^- or NO_3^- and varying ratio of ReO_4^- and NO_3^- in solution was mostly lepispheric and/or lenticular-shaped crystal structures, comprising of inter-grown thin disks or blades (Figure 2.4). Even though Al and Si source and ratios and reaction temperature used in this investigation were different from those in the study by Deng et al. (2006a), they reported similar morphology during hydrothermal synthesis of sodalite co-crystallized with

cancrinite in a starting solution with Si/Al <1.4. These results indicate that a reaction solution with Si/Al = 1 promotes the formation of sodalite.

2.4.5 Reaction Time Experiment

The crystal structure, morphology and anion incorporation into mixed sodalite were influenced by the amount and/or type of anions and the aging time. At the synthesis temperature of 90°C and 24-hour aging time, regardless of the concentration of the NO_3^- and ReO_4^- in the starting solutions, X-ray diffraction patterns indicate no morphological differences in the mixed sodalite (Figure 2.2). For the pure phase sodalites, (211) diffraction peak of the pure NO_3-sodalite shifted from a higher 2θ (24.3°) to a lower 2θ (23.8°) for the ReO_4-sodalite end-member consistent with larger *d*-spacing. The 24-hour aged mixed sodalite occurred mostly as lepispheric and/or lenticular-shaped particles (Figure 2.4 and Figure A.1, A, Supporting Information 1), whereas the 48 and 96-hour aged sodalites were characterized by euhedral hexagonal morphology (Figure A.1, B-C, Supporting Information 1). The 168-hour aged samples comprised of a mixture of lepispheric and hexagonal morphology (Figure A.1, D, Supporting Information 1).

2.4.6 Effect of Aging Time

Maintaining a constant ReO_4^-/NO_3^- ratio of 0.67:1 in the starting solutions, the influence of aging time on the crystal growth of mixed sodalite was investigated. The hydrothermal syntheses were conducted in an oven heated at 90°C for time intervals ranging from 24 to 168 hours (Table 2.1). XRD powder data confirm that predominantly mixed sodalites were formed with minor amounts of cancrinite. SEM images reveal distinct morphological changes of the sodalite crystals from 24 to 168 hour time interval.

The 24-hour aged mixed sodalites were characterized by the typical lepispheric morphology (Figure 2.4 and Figure A.1, A, Supporting Information 1), whereas the 48 and 96-hour aged exhibited euhedral hexagonal morphology indicative of highly crystalline phase(s) (Figure A.1, B-C, Supporting Information) (Deng et al., 2006b). However, the 168-hour aged samples were comprised of a mixture of lepispheric and hexagonal morphology (Figure A.1, D, Supporting Information 1).

Besides affecting the morphology and crystallinity, increased aging time also influenced the competitive inclusion of ReO_4^- into mixed sodalite phase(s). The 24 and 96-hour aged samples incorporated 67% and 49% more ReO_4^- respectively in comparison with the 168-hour aged samples (Figure A.2, Supporting Information 1). The 48 and 168-hour samples incorporated ReO_4^- at the same levels. Lastly, relatively high ReO_4^- content, euhedral crystal structures, and minor inclusion of up to 8% of cancrinite characterized the 96-hour aged samples, whereas the 168-hour samples contained 11% cancrinite, decreased ReO_4^- content in the crystal structure, and reduced crystallinity (Figure A.2, Supporting Information 1). The loss of ReO_4^- with increasing reaction time is consistent with the NO_3-sodalite phase being more stable than ReO_4-sodalite.

2.4.7 Effect of Anion Types

The type of anions present in the starting solutions containing a 1:1 molar ratio of Si/Al significantly affects the formation pathway of mixed ReO_4/NO_3-sodalite. In the study by Deng et al. (2006b) they reported that anions such as Cl^- and NO_2^- predominantly favor the formation of sodalite over cancrinite whereas NO_3^-, CO_3^{2-}, and SO_4^{2-} foster cancrinite formation. Particularly, they attributed the formation of NO_3-sodalite/cancrinite

phase to the Si/Al molar ratio, mineralization effect of the high NaOH concentration (up to 16 *M*), and the reaction time.

However, in our study, when ReO_4^- and NO_3^- were added simultaneously to the precursor solutions, the formation of the mixed sodalite was dictated largely in part by the 1:1 molar ratio of Si/Al, the NaOH concentration (1.25 *M*), the difference in ionic size, and hydration energy of both anions. For example, differences in their respective ionic radii (NO_3^- = 1.96 and ReO_4^- = 2.60 Å) and dehydration energies (300 and 330 kJ/mol) (Marcus, 1991; Moyer and Bonnesen, 1979a), appear to favor incorporation of the smaller NO_3^- anion. This suggests that the smaller β-cage is energetically more favorable than that formed by incorporation of the larger ReO_4^-. The preference of the sodalite structure for NO_3^- is shown in Figure 2.5 and Figure A.3 (Supporting Information 1). This is supported by a similar study by (Trill, 2002) of mixed halide (Cl^-/I^-) sodalites, where they reported that either single-phase sodalite containing about 90% of the dominant halide (Cl^-) was formed or phase separation occurred.

2.4.8 Competitive Incorporation of NO_3^- and ReO_4^- into Mixed Sodalite

The hydrothermal synthesis of mixed ReO_4/NO_3 sodalites requires a highly alkaline solution and thus OH^- anions compete with NO_3^- (OH^-/NO_3^- = 0.28 – 1.41) and ReO_4^- (OH^-/ReO_4^- = 0.14 – 1.41) for intercalation into the mixed sodalite lattice. However NO_3^- is strongly preferred over the OH^- anion, which in turn can significantly suppress ReO_4^- immobilization, should ReO_4^- concentration in the starting solutions be inadequate. Hence we added excess concentrations of ReO_4^- and NO_3^- to the starting solutions to provide adequate supply of both anions for mixed sodalite lattice formation. This competition of ReO_4^- and NO_3^- for the sodalite lattice can be written as follows:

$$(ReO_4^-)_s + (NO_3^-)_{aq} \underset{K_{NO_3}}{\overset{K_{ReO_4}}{\rightleftharpoons}} (ReO_4^-)_{aq} + (NO_3^-)_s \qquad (1)$$

where aq and s refer to the aqueous and solid phases, respectively. At equilibrium conditions, the selectivity factor (conditional equilibrium constant) K_{ReO_4-/NO_3-} is described by

$$K_{ReO_4-/NO_3-} = \frac{[NO_3\text{-}]_s}{[ReO_4\text{-}]_s} \cdot \frac{[ReO_4\text{-}]_{aq}}{[NO_3\text{-}]_{aq}}$$

where brackets denote the concentrations of solid and aqueous solution species in mole fractions. Thus, we can write

$$K_{ReO_4-/NO_3-} = \frac{M_{NO_3-(s)}}{M_{ReO_4-(s)}} \cdot \frac{M_{ReO_4-(aq)}}{M_{NO_3-(aq)}}$$

Herein $M_{ReO_4-(aq)} = \frac{[ReO_4^-]_{aq}}{[ReO_4^-]_{aq}+[NO_3^-]_{aq}}$ and $M_{NO_3-(aq)} = \frac{[NO_3^-]_{aq}}{[ReO_4^-]_{aq}+[NO_3^-]_{aq}}$ denote the mole fraction of perrhenate and nitrate in aqueous solutions and K_{ReO_4-/NO_3-} the selectivity of sodalite for ReO_4^- over NO_3^-.

Shown in Figure 2.5 is the plot of $\frac{M_{ReO_4-(s)}}{M_{NO_3-(s)}}$ versus $\frac{M_{ReO_4-(aq)}}{M_{NO_3-(aq)}}$, where the slope denoting the selectivity coefficient varied as the mole fraction of ReO_4^- incorporated into the mixed sodalite increased (Table insert in Figure 2.5). Even though K_{ReO_4-/NO_3-} nonlinearly increased from 0.02 to 0.93 with increasing mole fraction of ReO_4^- occluded in the sodalite phase, NO_3^- is still strongly preferred an estimated 30 ±2 times more than ReO_4^- for the sodalite lattice. Increasing selectivity was found for the NO_3-sodalite as ReO_4^- mole fraction in solution approaches 0.9, above which incorporation of ReO_4^- into the mixed sodalite becomes significant.

The large preference for NO_3^- in the sodalite cages implies that the smaller cage is energetically favored in the sodalite framework; however, this study and others also demonstrate the feasibility of pure ReO_4-sodalite formation in the absence of NO_3^- (Mattigod et al., 2006). The fact that the selectivity for ReO_4^- increases significantly with higher ReO_4^- concentration in the solid is indicative that the two anions do not form an ideal solid solution in sodalite. The smaller NO_3^- is preferably incorporated into the sodalite framework, eventually resulting in the onset of either domain formation or a phase separation at high ReO_4^- concentration. On the basis of the powder XRD data, it was difficult to observe domain formation with the exception of the small amounts of cancrinite (up to 10 wt.% on average). We find it unlikely that ReO_4^- is incorporated into the cancrinite phase for the following reasons: (1) the refined cell parameter for cancrinite is the expected value for the pure NO_3-cancrinite phase(s) reported in literature (Liu et al., 2005); (2) the cell parameter for sodalite increases with ReO_4^- incorporation; and (3) ReO_4^- solid phase concentration decreased with increasing cancrinite formation in the reaction time experiment.

The relation between the unit cell parameter and the concentration of ReO_4^- in the solid also suggests the formation of domains. For an ideal, homogeneous solid solution, Vegard's Rule states that the unit cell parameter should increase linearly with the ReO_4^- concentration (Trill et al., 2002). Although Vegard's Rule is an empirical relation, the significant deviation shown in Figure A.3 (Supporting Information 1) implies that ReO_4^- is not homogeneously distributed within the mixed sodalite. This is not surprising given the large difference in calculated ionic radii of ReO_4^- and NO_3^-. The findings in this

study suggest that the formation of mixed sodalite at 90°C is modulated by enthalpy requirements due to the different sizes of the sodalite cages.

Synthesis of mixed ReO_4/NO_3-sodalite over a range of ReO_4^-/NO_3^- in solution strongly favors the formation of the NO_3-sodalite phase(s). Increasing the reaction time increases the crystallinity of mixed sodalite with some loss of ReO_4^-. At ReO_4^- mole fractions in solution ≤0.9, NO_3^- incorporation is strongly favored, whereas at ≥0.9, ReO_4^- selectivity for the mixed sodalite becomes significantly enhanced. Neither the selectivity coefficient nor the unit cell parameter changes linearly with the relative concentration of the ReO_4-sodalite phase(s). We infer from this that the ReO_4/NO_3-sodalite does not form a homogeneous, ideal solid phase(s).

Results from recent study by Pierce et al. (2014) suggest that ReO_4^- and SO_4^{2-} were simultaneously incorporated into mixed-anion sodalite. Trill et al. (2003) also reported similar results in the synthesis of several guest-guest anion sodalites. These combined results suggest that feldspathoids can immobilize ^{99}Tc in the presence of other anions contained in the waste streams assuming their ionic radii are similar. Although the structure of feldspathoids allows for TcO_4^- incorporation into their frameworks (Pierce et al., 2014, submitted), our results reveal that ReO_4^-, a surrogate for TcO_4^-, was significantly intercalated into sodalite only when small, competing anions such as NO_3^- are present in very low concentrations (ReO_4^-/NO_3^- ~30:1) or completely absent. Under the subsurface conditions resulting from nuclear waste leaks or discharge, it is expected that NO_3^- anions with higher selectivity must be first exhausted prior to significant TcO_4^- incorporation into the sodalite structure.

2.5 Tables and Figures

This page is intentionally left blank

Table 2.1: Conditions for hydrothermal syntheses

Sodalite type	$NaReO_4$ (M)	$NaNO_3$ (M)	Aging Time (h)
NO_3-SOD*	0	1.765	24
0.002-SOD‡	0.177	1.588	24
0.003-SOD‡	0.353	1.412	24
0.006-SOD‡	0.706	1.059	24, 48, 96, 168
0.007-SOD‡	0.883	0.883	24
0.030-SOD‡	1.059	0.706	24
0.075-SOD‡	1.412	0.353	24
ReO_4-SOD**	1.765	0	24

‡Samples' ReO_4/NO_3 ratio

*NO_3-SOD represents sample containing 0% ReO_4

**ReO_4-SOD contains 100% ReO_4

Table 2.2: Refined powder X-ray data for mixed-anion sodalite

Structural Formula	*a*	R_{wp}
$Na_8[Al_6Si_6O_{24}](NO_3)_{1.99}$	8.9762(3) †	10.38
$Na_8[Al_6Si_6O_{24}](ReO_{4(0.01)}NO_{3(2.09)})$	8.9808(3)	9.20
$Na_8[Al_6Si_6O_{24}](ReO_{4(0.01)}NO_{3(2.06)})$	8.9795(3)	12.36
$Na_8[Al_6Si_6O_{24}](ReO_{4(0.03)}NO_{3(1.97)})$	8.9774(3)	11.90
$Na_8[Al_6Si_6O_{24}](ReO_{4(0.01)}NO_{3(2.17)})$	8.9794(3)	12.18
$Na_8[Al_6Si_6O_{24}](ReO_{4(0.06)}NO_{3(1.94)})$	8.9873(3)	15.98
$Na_8[Al_6Si_6O_{24}](ReO_{4(0.14)}NO_{3(1.86)})$	8.9987(5)	11.07
$Na_8[Al_6Si_6O_{24}](ReO_4)_{1.94}$	9.1535(1)	9.09

†The number in parentheses is estimated standard deviation (esd) in the same decimal place as the digit preceding it.

a – lattice parameter

R_{wp} - weighted agreement factor

Table 2.3: Chemical composition data for pure and mixed sodalite (mol/formula unit)

Formula of Structure	Na	Al	Si	ReO_4	NO_3
$Na_8[Al_6Si_6O_{24}](NO_3)_{1.99}$	7.91(6) †	6.00(8)	6.15(23)		1.99(3)
$Na_8[Al_6Si_6O_{24}](ReO_{4(0.01)}NO_{3(2.09)})$	8.05(17)	6.02(5)	6.03(12)	0.01	2.09(7)
$Na_8[Al_6Si_6O_{24}](ReO_{4(0.01)}NO_{3(2.06)})$	8.05(17)	6.02(5)	6.03(12)	0.01	2.06(3)
$Na_8[Al_6Si_6O_{24}](ReO_{4(0.03)}NO_{3(1.97)})$	8.05(17)	6.02(5)	6.03(12)	0.03	1.97(7)
$Na_8[Al_6Si_6O_{24}](ReO_{4(0.01)}NO_{3(2.17)})$	8.05(17)	6.02(5)	6.03(12)	0.01	2.17(2)
$Na_8[Al_6Si_6O_{24}](ReO_{4(0.06)}NO_{3(1.94)})$	8.05(17)	6.02(5)	6.03(12)	0.06	1.94(5)
$Na_8[Al_6Si_6O_{24}](ReO_{4(0.14)}NO_{3(1.86)})$	8.05(17)	6.02(5)	6.03(12)	0.14	1.86(1)
$Na_8[Al_6Si_6O_{24}](ReO_4)_{1.94}$	8.00(20)	5.97(4)	6.09(9)	1.94(3)	

†The number in parentheses is the standard deviation in the same decimal place as the digit preceding it.

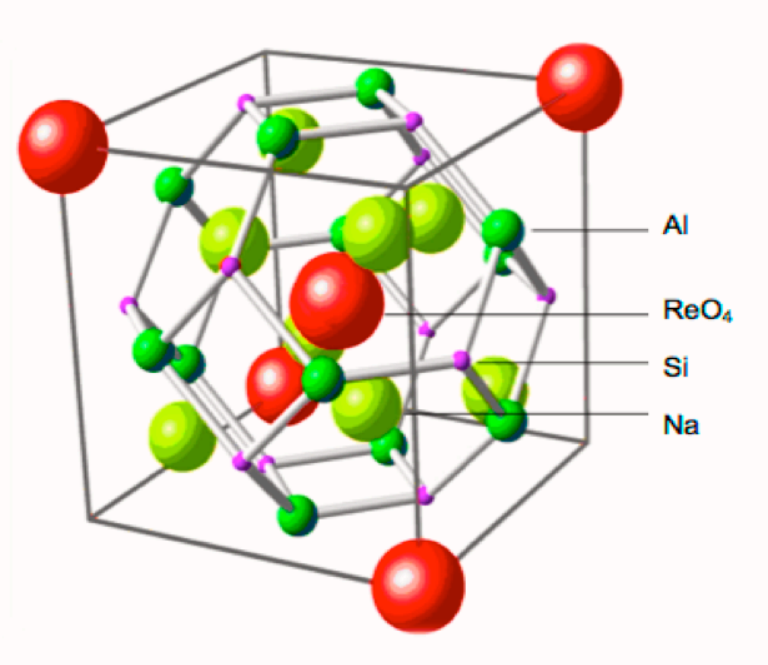

Figure 2.1: Face-sharing truncated octahedra of sodalite cages. The sodalite framework comprises of regularly alternating AlO_4 and SiO_4 tetrahedra with Al and Si residing at the corners of the truncated octahedral. Shown is pure ReO_4-sodalite phase(s) (Ashok et al., 2010)

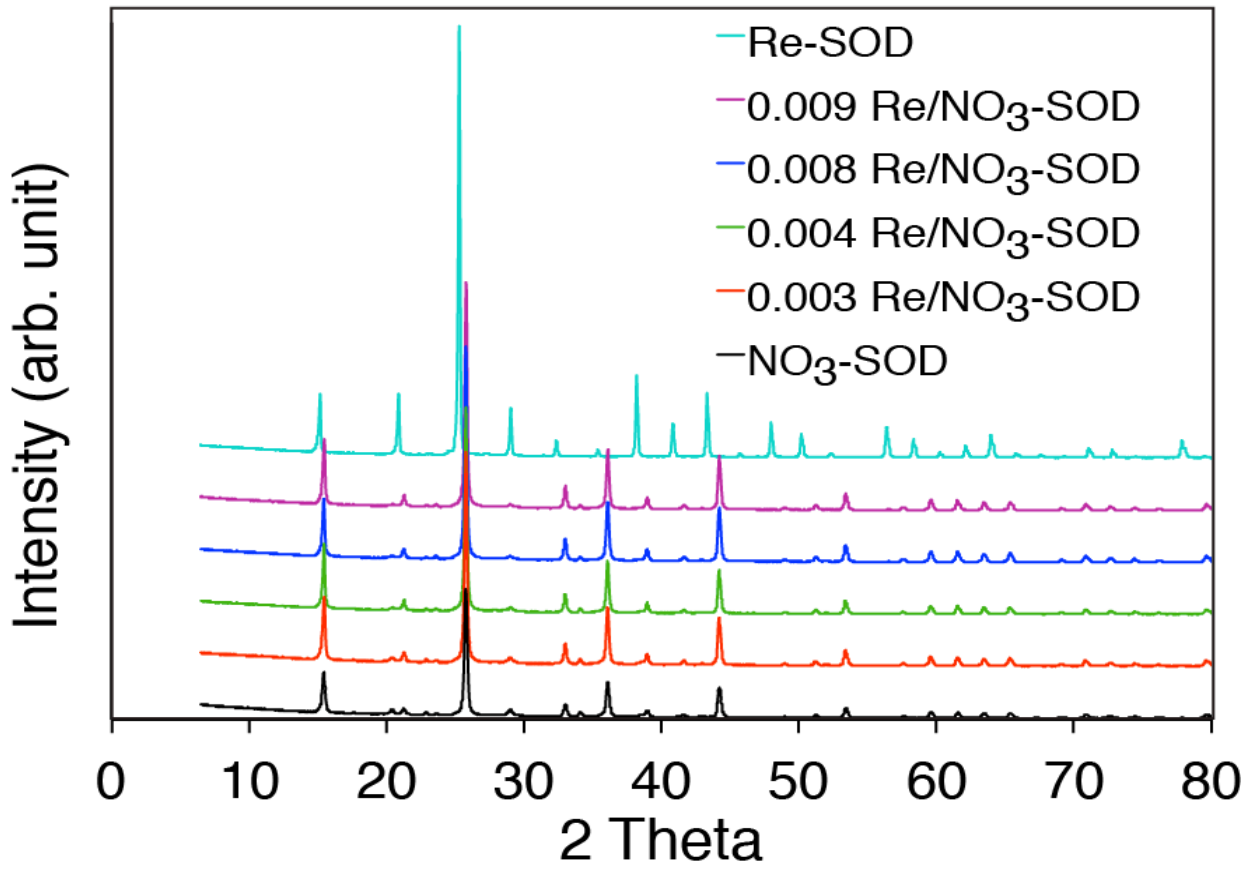

Figure 2.2: Refined powder X-ray spectra for selected mixed-anion sodalite

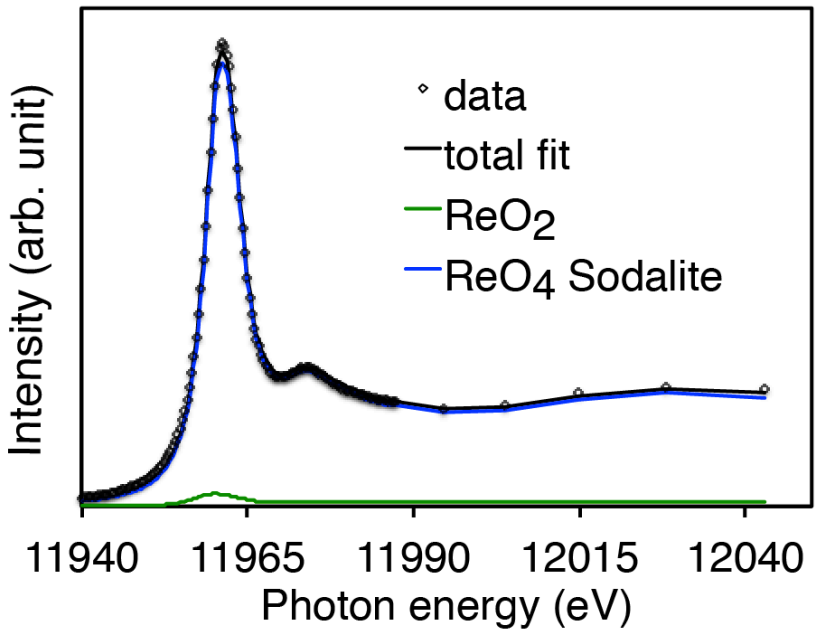

Figure 2.3: X-ray absorption spectral data for ReO_4/NO_3-sodalite assemblage; Data are represented by dots, and the fit is shown by the black line. Results indicate Re(VII) oxidation state.

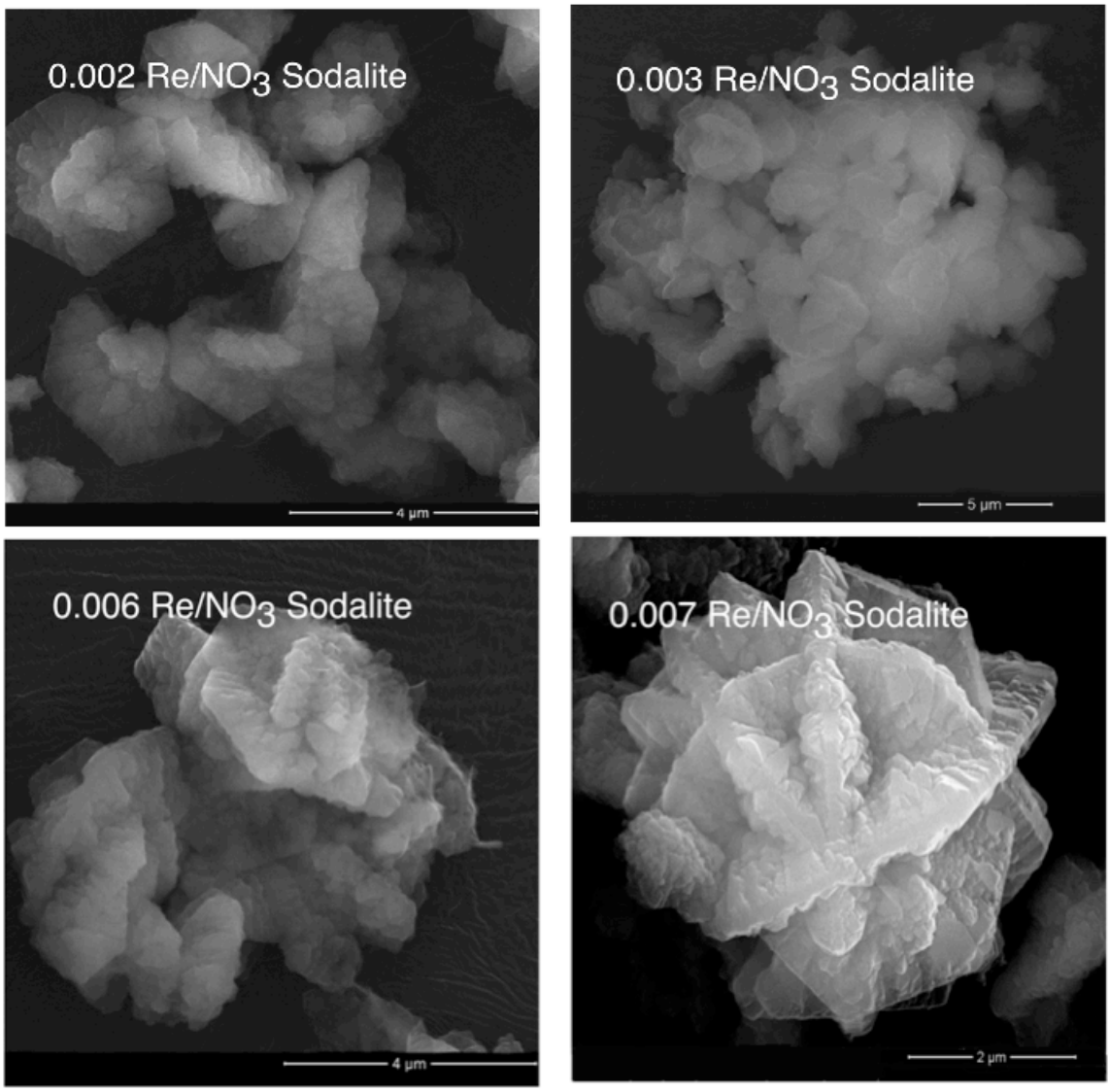

Figure 2.4: SEM micrographs of Re/NO_3-sodalites (0.002 – 0.007 molar ratios) formed in the presence of varying $NaReO_4/NaNO_3$ ratio in solution.

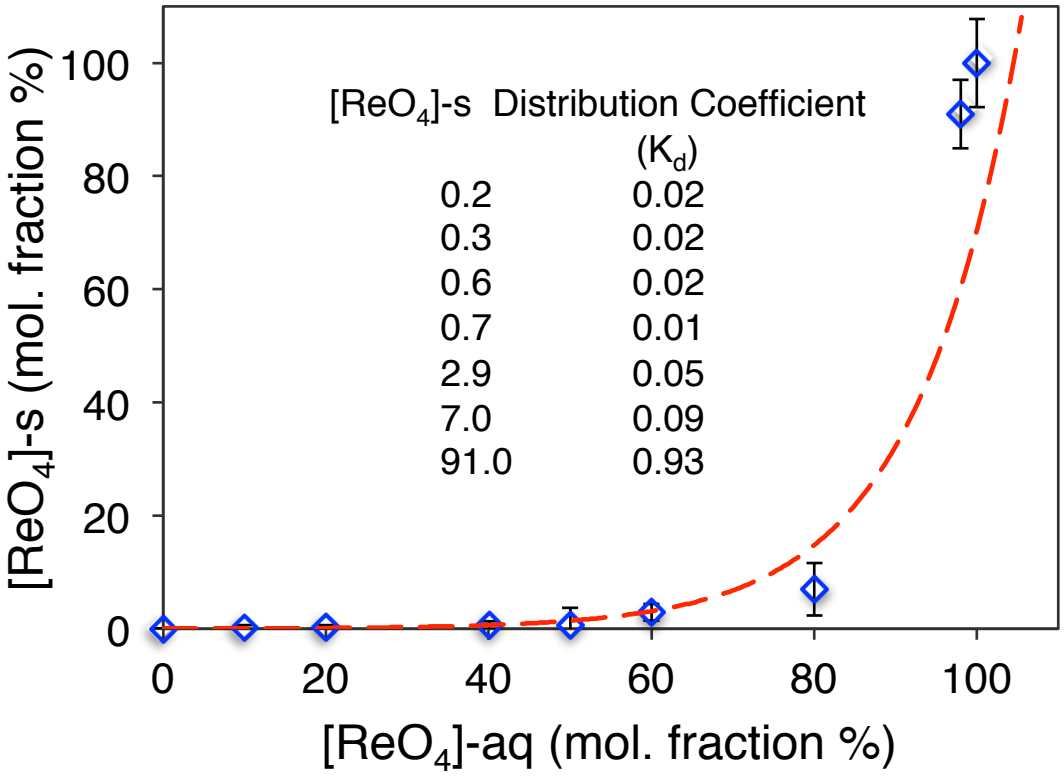

Figure 2.5: Selectivity graph for rhenium incorporation into ReO_4/NO_3 sodalite; generally more than 90% of sodalite cages are filled with oxyanions. Insert shows the selectivity coefficients as a function of ReO_4^- mole fraction in the final solid

Appendix

Supporting Information

This section contains information on XANES analysis, additional SEM micrographs of mixed sodalite aged at different time interval, figures showing the variation of ReO_4^- concentrations with time and lattice parameter

A.1 X-ray Absorption Near Edge Structure (XANES) Spectroscopy

The spectra fitting were performed as previously described by Lukens et al. (2005, 2007) by inclusion of all reference spectra. Thus, the final fit includes only the reference spectra that have non-zero contributions to the fit. The improvement to the fit due to the contribution of the reference spectra was evaluated using the random error test (*F*-test), which is the likelihood that the improvement in the fit due to inclusion of the standard spectrum is due to noise in the data. If $p < 0.05$, then the data supports the hypothesis that a given component is present (improvement is > 2σ of the fit), and if $p < 0.01$, then the data strongly supports the hypothesis (improvement is > 3σ of the fit).

This section has been submitted as supporting information to a technical journal: Dickson, J.O., Harsh, J.B., Flury, M., Lukens, W.W., Pierce, E.M. (2014), Competitive incorporation of perrhenate and nitrate into sodalite. *Environ. Sci. Technol.* (submitted)

Table A.1: Result of XANES spectra fitting for ReO_4/NO_3-sodalite

Sample‡‡	ReO_2	p*	ReO_4-sodalite	p*
0.002-SOD	0.11(5)†	0.065	0.89(4)	<0.001
0.006-SOD	0.04(6)	0.560	0.96(4)	<0.001
0.007-SOD	0.05(6)	0.468	0.95(4)	<0.001

†The number in parentheses is the standard deviation in the same decimal place as the digit preceding it.

*p is the usual p-value

‡‡Samples' ReO_4^-/NO_3^- ratio

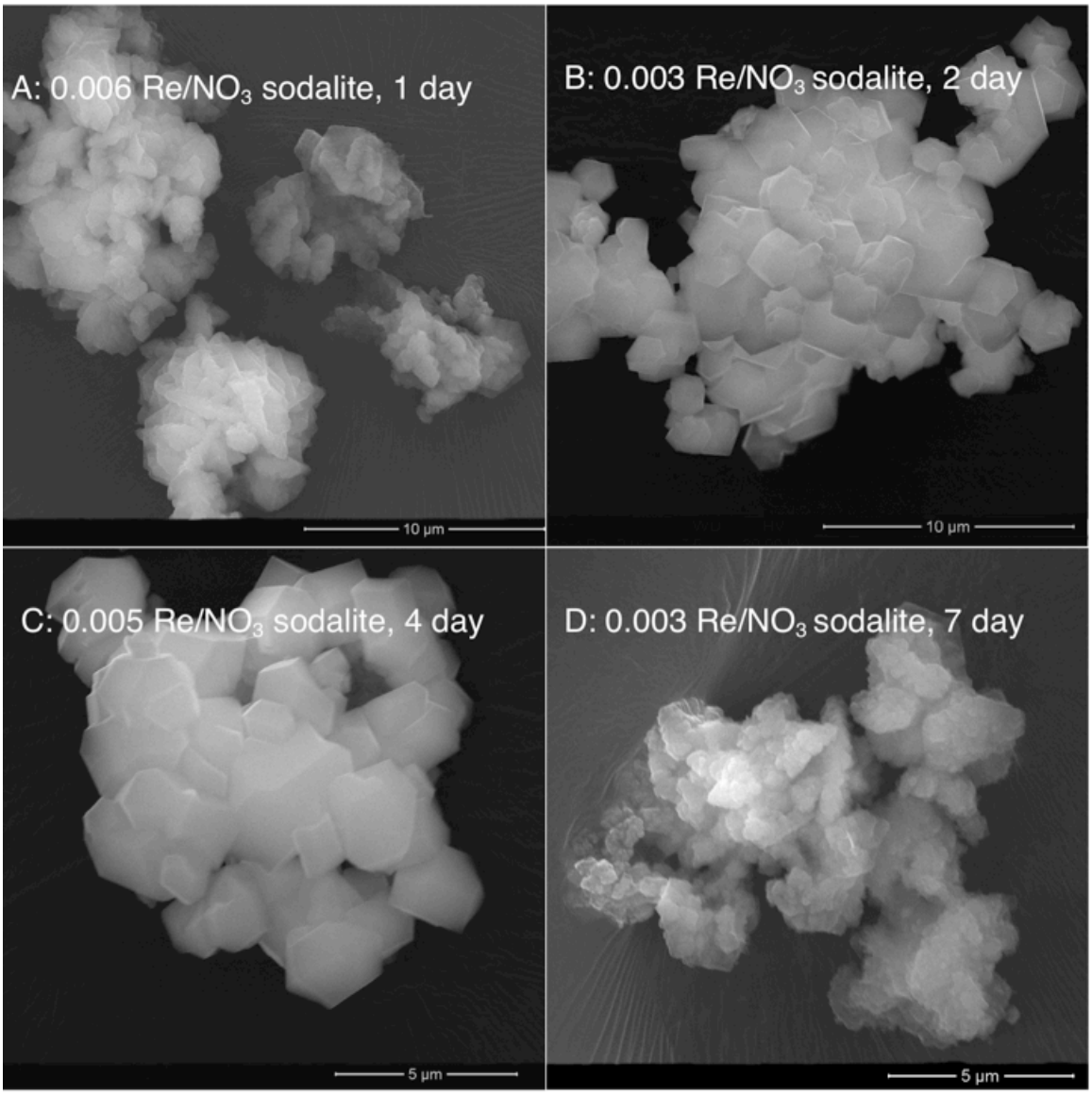

Figure A.1: SEM micrographs of 0.003 – 0.006 Re/NO_3-sodalites formed in 0.67 ReO_4^-/NO_3^- ratios in solution over 24 – 168 hour aging time.

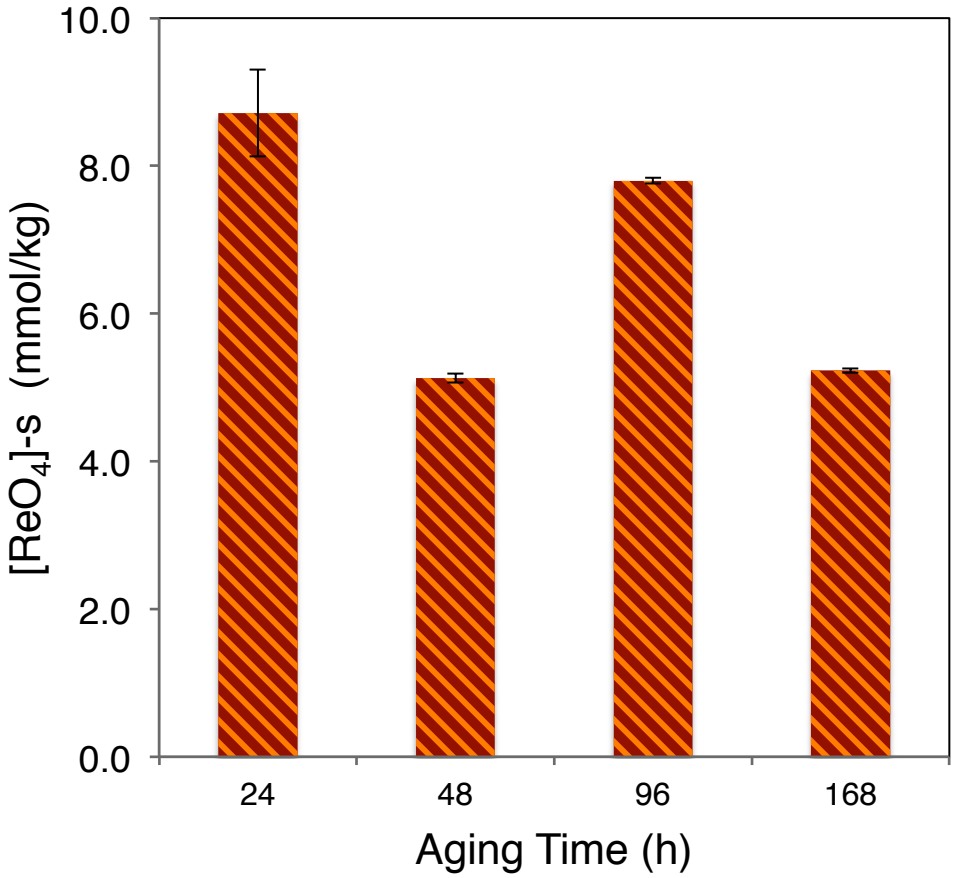

Figure A.2: Variation of ReO_4^- concentration in mixed sodalites with aging time in solution with 0.67 ReO_4^-/NO_3^- ratio.

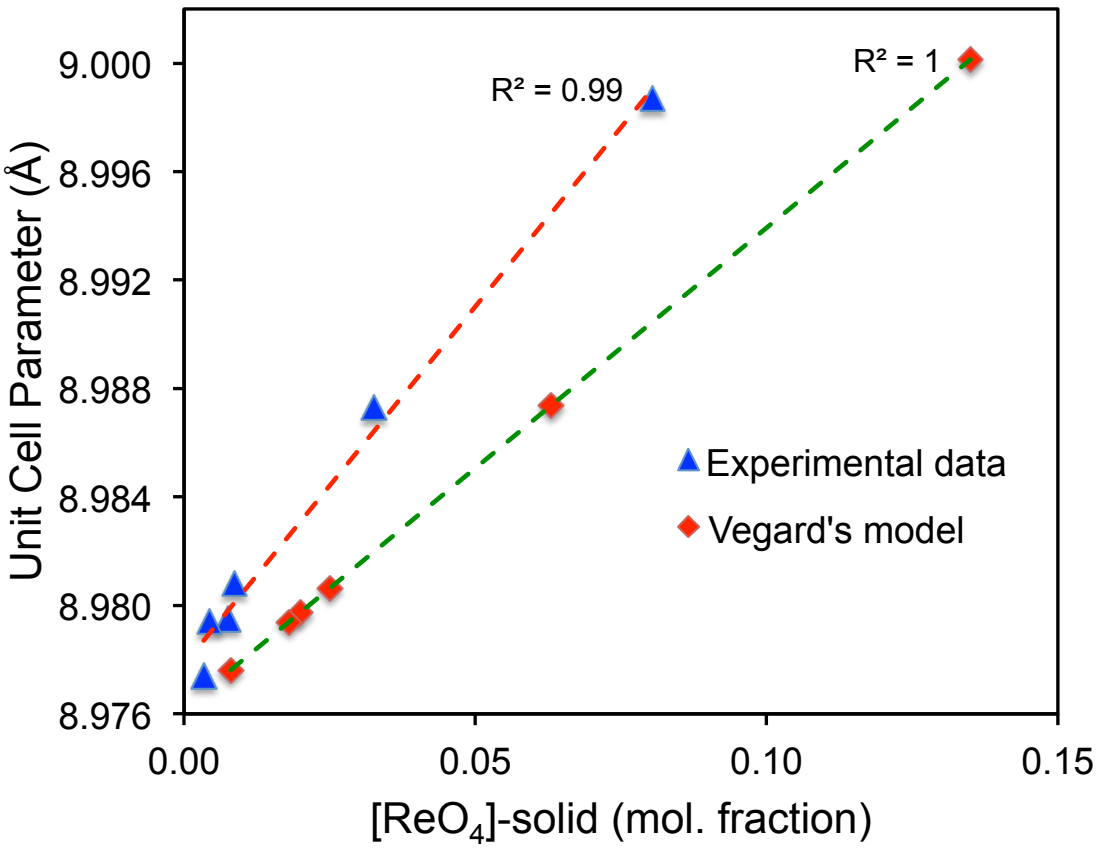

Figure A.3: Dependence of the unit cell parameter on ReO_4^- concentration in ReO_4/NO_3-sodalite; Data predicted by Vegard's model are compared with experimental value.

Chapter 3

Perrhenate Incorporation into Binary Mixed Sodalites: The Role of Anion Size and Implications for Technetium-99 Sequestration

3.1 Abstract

Perrhenate (ReO_4^-), as a TcO_4^- analogue was incorporated into mixed-anion sodalites from binary solutions containing ReO_4^- and a competing anion X^{n-} (Cl^-, CO_3^{2-}, SO_4^{2-}, MnO_4^-, or WO_4^{2-}). Our objective was to determine the extent of solid solutions formation and the dependence of competing ions selectivity on ion size. Using equivalent aqueous concentrations of the anions (ReO_4^-/ X^{n-} molar ratio = 1:1), we synthesized mixed-anion sodalites from zeolite and NaOH at 90°C for 96 hours. The resulting solids were characterized by bulk chemical analysis, X-ray diffraction, scanning electron microscopy, and X-ray absorption near edge structure (XANES) spectroscopy to determine the crystal structure, chemical composition, and morphology, and to confirm the rhenium (Re) oxidation state.

This chapter has been submitted to a technical journal: Dickson, J.O., Harsh, J.B., Lukens, W.W., Pierce, E.M. (2014), Perrhenate incorporation into binary mixed sodalites: The role of anion size and implications for technetium-99 sequestration. *Chem. Geol.* (submitted)

Rhenium in the solid phase occurred predominately as $Re(VII)O_4^-$ in the sodalite, which has a primitive cubic pattern in the space group $P\bar{4}3n$. The refined unit-cell parameters of the mixed sodalites ranged from 8.88 to 9.15 Å and showed a linear dependence on the size and mole fraction of the incorporated anion(s). The ReO_4^- selectivity, represented by its distribution coefficient, increased in the following order: $Cl^-<NO_3^-<MnO_4^-$ and $CO_3^{2-}<SO_4^{2-}<WO_4^{2-}$ for the monovalent and divalent anions respectively. The relationship between the ReO_4^- distribution coefficient and competing anion size was nonlinear. When the difference in ionic radius (DIR) between ReO_4^- and X^{n-} ($1 \leq n \leq 2$) was greater than ~12%, then ReO_4^- incorporation into sodalite was insignificant. The results imply that anion size is the major factor that determines sodalite anion compositions and that ReO_4^- is likely to serve as a suitable analogue for TcO_4^- where Tc(VII) is the stable oxidation state.

3.2 Introduction

The application of versatile porous framework materials (feldspathoids) as a selective medium for sequestration of key anionic radionuclides is of paramount importance to the nuclear waste industry. Furthermore, advanced knowledge of factors governing anion selectivity in feldspathoids is critical for their potential application in anion-sequestration processes (Custelcean and Moyer, 2007). The safe disposal of nuclear waste generated by the nuclear fuel cycle remains one of the most challenging and potentially costly environmental endeavours facing the nuclear energy industry. Additionally, disposal of reprocessed waste generated as a result of the Cold War remains a challenge for numerous industrialized nations (Ewing, 1999).

While glass (borosilicate) waste forms have been employed to immobilize high level nuclear waste (HLW) from nuclear weapons programs and spent nuclear fuel (SNF) from commercial nuclear power plants, ceramic (zirconolite, apatite, synroc, pyrochlore) and glass ceramic (titanite, celsian, zirconolite, silicotitantates, and apatitic) waste forms have been proposed for immobilization of defense HLW and spent nuclear fuel (Weber et al., 2009). Vitrification processes are currently employed to treat commercial HLW at West Valley site (New York) and defense HLW at DOE Savannah River site (Aiken, South Carolina); while at the DOE Hanford site (Washington), construction of a vitrification plant is underway to immobilize defense HLW (Weber et al., 2009).

It has been shown that percolating pore water reacts with glass waste to form more stable secondary phases, including zeolite (analcime), smectite (Na-beidellite), and feldspathoids (Inagaki et al., 2002; Mattigod et al., 2002). As products of chemical weathering, these secondary mineral phases can potentially retain radionuclides

released from corroding vitreous waste forms in their frameworks, thereby controlling the fate and transport of key radionuclides in the environment.

Feldspathoids such as cancrinite and sodalite have crystalline microporous framework structures. They can be represented by the general formula: $A_8[TO_4]_6X_2$ where T is Al and/or Si and, A and X are monovalent or divalent cations and anions, respectively (Taylor and Henderson, 1978). Sodalite consists of corner sharing SiO_4 and AlO_4 tetrahedra constructed into four and six-membered rings that form the cuboctahedral cages referred to as sodalite β-cages. The sodalite framework can be considered as a space-filling arrangement of the sodalite β-cages directly linked via the six-membered rings to form the semi-condensed sodalite structure. In the center of the cage is an anion that is tetrahedrally coordinated to four cations, forming A_4X clusters (Trill, 2002).

Feldspathoids with guest ions in their structure have been widely studied (Johnson et al., 1999). Most studies have been devoted to mixed cation substitutions in sodalite frameworks (Brenchley and Weller, 1994; Stein et al., 1992) and to single anion sodalites (Weller and Wong, 1989; Weller et al., 1990), but the substitution of multiple guest anions in mixed sodalite phases is not well understood. An understanding of sodalite selectivity for anionic species of varying sizes is important for elucidating anion substitution in mixed sodalite with more complex structures, especially those sodalites containing key anionic radionuclides ($^{99}TcO_4^-$, $^{129}I^-$, $^{75}SeO_4^{2-}$).

While it seems likely that $^{99}TcO_4^-$ would be sequestered by feldspathoid phases during glass corrosion, previous studies of waste glass weathering show that ^{99}Tc is released congruently with boron (Bibler and Jurgensen, 1988). This contradiction

illustrates the significant gaps in our current understanding of the role of sodalite selectivity as a driving force for controlling anion incorporations into the structure. Previous work with NO_3/ReO_4-sodalites suggests that selectivity might be anion size-dependent (Dickson et al., 2014, submitted), but no experimental evidence exists that demonstrates the selectivity of different ions for incorporation into sodalites Therefore, we investigated the competitive incorporation of ReO_4^- into mixed anion-bearing sodalite in the presence of these competing anions (X^{n-}) ranging in size and charge: Cl^-, CO_3^{2-}, SO_4^{2-}, MnO_4^-, and WO_4^{2-}.

This study highlights the dependence of selectivity on ion size and charge. Additionally the variation of the sodalite structural parameter as a function of composition (anion mixing) will shed light on the extent of anion incorporation into mixed sodalites formed in environmentally relevant conditions such as subsurface and engineered wastes, vitrification products, and materials formed by chemical weathering.

3.3 Materials and Methods

3.3.1 Rhenium as Analogue for Tc

We used Re as a nonradioactive analogue for Tc. Under aerobic (oxic) conditions both elements occur as oxyanions (ReO_4^- and TcO_4^-), which have similar metal oxygen bond lengths (Tc–O = 1.702 Å and Re–O = 1.719 Å) and ionic radii (TcO_4^- = 2.52 Å and ReO_4^- = 2.60 Å)(Icenhower et al., 2010; Marcus, 1991; Moyer and Bonnesen, 1979b)

3.3.2 Hydrothermal Mineral Synthesis

Mixed-anion sodalites with ReO_4^- and one other anion (X^{n-}) were hydrothermally synthesized based on modification of a method previously described by Liu and

Navrotsky (Liu and Navrotsky, 2007): Sodium hydroxide (Alfa Aesar) was mixed with zeolite 4A ($Na_{12}Al_{12}Si_{12}O_{48}$ xH_2O, W.R Grace & Co.) and sodium salts of the appropriate anions. The zeolite supplied a 1:1 molar ratio of Si/Al. The mixed sodalites were synthesized in a 60-mL Teflon digestion bomb filled with 20 mL of de-ionized water, one gram of NaOH pellets (1.25 *M* NaOH) and 0.5 g of zeolite. To these basic solutions, 0.88 *M* of $NaReO_4$ was added and 0.88 *M* of Cl^-, CO_3^{2-}, SO_4^{2-}, MnO_4^-, or $WO_4^{2-}$was added as the competing anion. The rationale for the concentrations used in this experiment was that we wanted to produce pure sodalite phases and to determine anion selectivity in a mixed system. All chemical reagents were used as received. The bombs were capped, and aged for 96 hours in a 90°C oven. After decanting the basic supernatant solutions the solid precipitates were washed three times with deionized water (0.054×10^{-3} dSm^{-1}) by centrifugation. The solids were dialyzed in deionized water until the electrolytic conductivity was ≤0.01 dSm^{-1}, dried for 24 hours, and weighed. Solid yield after dialysis ranged from 0.5 to 0.6 g.

3.3.3 Powder X-ray Diffraction

X-ray diffraction data were obtained with a Panalytical Xpert Pro diffractometer (XRD) scanning at 1.5°/min over 5 – 90° 2θ. We used CoKα radiation (λ = 1.789010 Å) and an X'Celerator silicon strip detector equipped with an Fe filter. Scans used ¼° fixed divergence slits and ½° anti-scatter slit. “Jade” and/or HighScore Plus software, and the ICDD database were used for mineral identification. Rietveld refinements of the XRD data were performed in High Score Plus and/or GSAS with EXPGUI interface (Toby, 2001) using the reported structures of the following phases: $Na_8(AlSiO_4)_6(NO_2)_2$ (Buhl and Lons, 1996), $Na_8(AlSiO_4)_6(ReO_4)_2$ (Mattigod et al., 2006), and

$Na_6Ca_{1.5}(AlSiO_4)_6(CO_3)_{1.5}(H_2O)_{1.75}$ (Hackbarth et al., 1999). The following parameters were allowed to vary: the background (8 parameters), unit cell, Na position, Re/anion occupancy, peak shape (5 parameters: U, V, W, and two peak shape parameters), overall thermal parameter (B), and preferred orientation.

3.3.4 X-ray Absorption Near Edge Structure (XANES) Spectroscopy

Powdered sodalite samples were mixed with boron nitride and mounted on an aluminum holder with Kapton windows. The XANES spectra were obtained at the Stanford Synchrotron Radiation Lightsource (SSRL) using the 11-2 beamline equipped with a Si (220) double crystal monochromator (ϕ = 90 crystals) detuned 50% to reduce the harmonic content of the beam. The spectra from 0.2 keV below to 10 keV above the Re L_2-edge (11.959 keV) were collected either in transmission mode using nitrogen-filled ion chambers or fluorescence mode using a 100-element Ge detector and corrected for detector dead time. We converted raw data to spectra and normalized with SixPack and Artemis (Ravel and Newville, 2005). Normalized XANES spectra were fit using standard spectra in the locally written program 'fites', which utilizes a non-linear least squares fitting data. Two reference spectra, ReO_2, and pure ReO_4-sodalite, were used for data fitting. The sample XANES spectra were allowed to vary in energy during fitting and the spectral resolution is 7 eV based on the width of the white line at the Re L_2-edge.

3.3.5 Electron Microscopy

Scanning electron micrographs (SEM) were obtained with platinum-palladium sputter-coated powder samples. The coated powder samples were examined under field emission scanning electron microscope (FESEM) (FEI Quanta 200F, FEI Co., Hillsboro,

OR). Particle size distributions were determined by dynamic light scattering (DelsaNano C Particle Analyzer, Beckman Coulter Inc., Brea, CA) equipped with a 633 nm Helium-Neon laser.

3.3.6 Chemical Analysis

The powder samples digested in 3% nitric acid were analyzed for Na concentration by atomic emission and absorption spectrophotometry (Varian 220 Flame Atomic Absorption Spectrometer, Varian Ltd., Mulgrave, Australia). The Si, Al, Mn, W, and Re concentration in the solids were determined by inductively coupled plasma-mass spectrometer (Agilent 7700 ICP-MS, Santa Clara, CA) and concentrations of Cl^- and, SO_4^{2-} by ion chromatography (HPLC-10Ai, Shimadzu Inc., Canby, OR). Total carbon concentration was determined by dry combustion from TruSpec C/N analyzer (Leco Corporation, St. Joseph, MI) equipped with a high temperature combustion method and infrared detection technique.

3.4 Results

3.4.1 Synthesis Product Morphology

The SEM photographs of the mixed-anion sodalites are shown in Figure 3.1. The mixed-anion sodalites formed in the presence of Cl^-, CO_3^{2-}, MnO_4^- and WO_4^{2-} were hexagonal crystallites (Figure 3.1A-B, D-E). The observed morphology differs from the lepispheric morphology reported by Deng et al. (2006b) for precipitates formed from simultaneous additions of two or more anions (Cl^-, NO_2^-, NO_3^-, CO_3^{2-}, SO_4^{2-}, PO_4^{3-}) to starting solutions of Na hydroxide, aluminate, and silicate. In contrast, our experiments used zeolite as Al and Si source. The crystalline solids formed in the presence of SO_4^{2-}

anions were dominated by lepispheric and lenticular-shaped crystal structures, comprised of inter-grown thin disks or blades (Figure 3.1C). The observed ReO_4/SO_4-sodalite morphology was similar to those reported by Deng et al, (2006) for precipitates formed in binary or multi-anion solutions. Particle size measurements data for the mixed-anion sodalites are presented in Table 3.1. The particle sizes were consistent with those reported by Missimer and Rutherford (2013) for similar phases. Differences among the mixed-anion sodalite phases are due either to the degree of crystal growth or the amount of agglomeration.

3.4.2 Composition Analysis

The chemical composition of the synthesis products is shown in Table 3.2. The mixed-anion sodalites contained from 0.02 – 1.90 mole ReO_4^- and 0.04 – 2.10 mole of X^{n-} per formula unit. The sodalites synthesized in the presence of ReO_4^- and Cl^-, CO_3^{2-}, or SO_4^{2-} incorporated negligible amounts of ReO_4^-. In contrast, the sodalite cages exhibited strong preference for ReO_4^- over WO_4^{2-} with ~95% ReO_4^- occupancy of available sites. Further evidence of ReO_4^- incorporation into sodalite is shown in the energy-dispersive X-ray spectroscopy (EDS) patterns (Figure 3.2). Perrhenate was best incorporated into the ReO_4/MnO_4- and ReO_4/WO_4-sodalites whereas insignificant incorporation occurred for the ReO_4/Cl-, ReO_4/SO_4- and ReO_4/CO_3-sodalites.

3.4.3 Mineral Structure

The calculated XRD patterns obtained from the Rietveld refinements of the mixed-anion sodalites are displayed in Figure 3.3. The refined lattice parameter, (*a*) and index of agreement (χ^2) for the mixed-anion sodalites are shown in Table 3.3. The space group $P\bar{4}3n$ was adopted for the mixed-anion sodalite with (*a*) ranging from 8.8885(2) to

9.1527(1) Å. The Rietveld refinements indicate minor amounts of cancrinite (<2 wt%) were formed along with the dominant sodalite phase(s).

3.4.4 Rhenium Oxidation State

The spectra fitting were performed as described by Lukens et al. (2007). The Re L_2-edge XANES data were fit using only the spectra of ReO_2(s) and ReO_4-sodalite. The spectrum ReO_4/MnO_4-sodalite is presented in Figure 3.4. In the mixed-anion sodalites, the spectrum of ReO_4-sodalite contributes significantly (≥92%) to the fit and only in the presence of Cl^- does the spectrum of ReO_2 contribute significantly to greater than 2σ of the fit (Table 3.4). Thus, the ReO_4^- species is considered the dominant rhenium species in these solid phases.

3.5 Discussion

3.5.1 Incorporation of ReO_4^- in the Presence of Competing Anion (X)

Using an equal concentration of ReO_4^- and X^{n-} in the starting solutions, we synthesized five mixed-anion sodalites and tested the hypotheses that ionic sizes and mole fraction determine the lattice parameter and that ion size and charge drive the selectivity between the two anions.

As the ionic radius increases in the following series: $Cl^-<CO_3^{2-}<SO_4^{2-}<MnO_4^-<WO_4^{2-}$ the selectivity of ReO_4^- for the mixed sodalite linearly increased (Figure 3.5), consistent with the linear expansion of the cages from the ReO_4/Cl-sodalite to the ReO_4/WO_4-sodalites. Vegard's Rule [$a_{AB} = a_A(M_A) + (1-M_A)a_B$] predicts a linear relationship between the crystal lattice parameter of solid solutions (a_{AB}) and a weighted average size based on concentrations (M_A, $1-M_A$) and radii of the

constituent elements *A* and *B*. The rule is expected to hold for well-mixed solid solutions; however, substantial differences in anion size may lead to phase separation and differences in charge to incomplete cage filling.

The larger the difference in size between ReO_4^- and the competing anion (Table 3.5), the more likely are the deviations from their random distribution in the sodalite lattice leading to noncompliance with Vegard's Rule. Similarly, anions of greater charge will not occupy all cages. Because negligible amounts of ReO_4^- were incorporated into the Cl-, CO_3-, and SO_4-sodalites, the observed linear fit due to the size of the three ions does not imply phase separation. Moreover the mixed sodalites that contained significant amounts of each anion also fit the line generated by Vegard's Rule, suggesting that the ReO_4-sodalites containing MnO_4^- or WO_4^{2-} are well-mixed solid solutions (Figure 3.5). Only CO_3^{2-} deviates significantly from the line and this is likely because only half the cages can be occupied to maintain charge balance.

The inability to form mixed sodalites containing significant ReO_4^- in the presence of Cl^-, CO_3^{2-}, and SO_4^{2-} is due the large size difference between ReO_4^- and the competing anions. According to Hume-Rothery Rules, the following conditions favor solid solution formation: similarity in the resulting crystal structure and ion valency, electronegativity and size. Sodalite cages can host anions of varying size due to cooperative tilting and deformation of the frameworks up to a point. Trill et al. (2003) state that the difference in anion size may not exceed 15%, because of excessive strain on the sodalite framework (Trill et al., 2003). This behavior is confirmed in our system as shown in Figure 3.6 where anion selectivity is plotted against the difference in ionic radii (DIR) of solvent A (r_A) and solute B (r_B) where:

$$\mathrm{DIR}\ (\%) = \left(\frac{r_A - r_B}{r_B}\right) \times 100$$

As DIR increases from 2.7% in the ReO_4/WO_4-sodalite to 51.2% in the ReO_4/Cl-sodalite, the ReO_4^- distribution coefficient exponentially declines from 3.73 to 0.02. When the difference in ionic radii (DIR) between ReO_4^- and the competing anion exceeds 15%, the concomitant inclusion of both anions would sufficiently distort the mixed-anion sodalite cages, resulting in the exclusion of the larger anion from the cages. This is manifested in the preferential formation of mostly Cl-, CO_3- and SO_4-sodalites containing minor amounts of enclathrated ReO_4^-. Although the DIR for ReO_4/SO_4 (13%) and ReO_4/WO_4-sodalites (2.7%) should favor the formation of mixed sodalite solid solutions, the distribution coefficient shows a clear preference for SO_4^{2-} and ReO_4^- respectively. In the case of SO_4^{2-}, DIR is close to 15%, indicating that this difference is still large enough to strongly favor the smaller anion. For WO_4^{2-}, the difference in charge and inability to fill all cages with either ReO_4^- or WO_4^{2-} may explain ReO_4^- preference.

3.6 Environmental Implications for ^{99}Tc Immobilization.

In this study five mixed-anion sodalites containing extra-framework species were synthesized and characterized. The selectivity for intra-lattice anions of the products was highly dependent on the size and, to a lesser extent, the charge of the competing anion. The results of our study suggest that similarity in ionic radius (DIR of ≤15%) and charge (ionic potential) promote the competitive incorporation of ReO_4^- into the mixed-anion sodalite (Figure 3.6 and Table 3.5). Selectivity of ReO_4^- for the mixed-anion sodalite was found to increase in the series as follows:

$Cl^- < CO_3^{2-} < NO_3^- < SO_4^{2-} << MnO_4^- < WO_4^{2-}$.

The findings in this study have implications for the fate and transport of $^{99}TcO_4^-$ in subsurface sediments assuming that its chemical behavior can be well approximated by ReO_4^-. Firstly, the formation of a ReO_4/MnO_4-sodalite solid solution implies that ReO_4^- is a suitable analogue for TcO_4^-. Like TcO_4^-, MnO_4^- shares a similar size, ionic potential, and electronegativity with ReO_4^- (Table 3.5). The solid solution is consistent with Vegard's Rule and the distribution coefficient for ReO_4^- was unity, implying nearly equal selectivity for MnO_4^- and ReO_4^- during the formation of sodalite. The same is likely to be true for TcO_4-sodalite. Secondly, our results also suggest that neoformed feldspathoid minerals, such as sodalite, can incorporate ^{99}Tc as TcO_4^-, but smaller competing anions with DIR >12% will be preferred. Unfortunately, in many cases where environmental conditions are conducive for feldspathoid formation, the waste solutions may also contain high concentrations of such competing anions.

One limitation of our results is that sodalite synthesis occurred in a closed system. In open, free-flowing systems, the smaller anions may become depleted leaving TcO_4^- to be incorporated later in the reaction sequence. Additionally, our experiments were designed specifically to form sodalite phase because of the ability of its cages to sequester large ions such as TcO_4^-. In other systems, neoformed mineral phases could include zeolite, nosean, and nepheline. It has been reported that NO_3^- will sequester into cancrinite and SO_4^{2-} into nosean; whereas Cl^- and ReO_4^- will be incorporated into mixed sodalite (Pierce et al., 2014). Thus, at the comparatively low concentrations of TcO_4^- (10^{-6} to 10^{-4} M) expected in most nuclear waste streams, TcO_4^- could intercalate into the mixed-anion sodalite phases after other competing anions have been

selectively sequestered into their respective neoformed mineral phases. Further work is needed in open systems, with a greater range of conditions, and at realistic ^{99}Tc concentrations to mimic waste-impacted subsurface sediments and managed waste streams to determine if mixed-anion sodalites may be relevant sequestering phase(s).

3.7 Tables and Figures

This page is intentionally left blank

Table 3.1: Particle size data (mean volume distribution) for mixed-anion sodalites.

Percentile	Re/Cl-SOD Size (μm)	Re/CO_3-SOD Size (μm)	Re/SO_4-SOD Size (μm)	Re/MnO_4-SOD Size (μm)	Re/WO_4-SOD Size (μm)
10	0.250	0.281	0.137	0.192	0.173
25	0.446	0.587	0.271	0.459	0.436
40	0.794	1.231	0.534	1.103	1.101
50	1.172	2.015	0.841	1.983	2.033
60	1.72	3.304	1.324	3.574	3.777
75	3.08	6.93	2.62	8.69	9.49
85	4.54	9.43	4.12	15.72	17.63
95	6.71	15.11	6.49	28.54	32.61

Table 3.2: Mixed-anion sodalite chemical composition data (mol/formula unit).

Structural Formula	Na	Al	Si	Re/X	ReO_4	X
$Na_8[Al_6Si_6O_{24}](Cl_{(2.1)}ReO_{4(0.003)})$	7.96 ±0.16	6.00 ±0.05	6.06 ±0.11	0.00	0.003 ±0.001	2.14 ±0.07
$Na_8[Al_6Si_6O_{24}](CO_{3(1.0)}ReO_{4(0.02)})$	8.00 ±0.30	6.01 ±0.11	6.00 ±0.10	0.02	0.021 ±0.005	1.01 ±0.1
$Na_{7.6}[Al_6Si_6O_{24}](SO_{4(0.96)}ReO_{4(0.08)})$	7.61 ±0.07	6.02 ±0.07	6.08 ±0.07	0.08	0.08 ±0.002	0.958 ±0.12
$Na_8[Al_6Si_{5.9}O_{24}](MnO_{4(1.1)}\ ReO_{4(0.97)})$	8.09 ±0.17	6.09 ±0.05	5.92 ±0.02	0.89	0.965 ±0.02	1.09 ±0.03
$Na_{7.9}[Al_6Si_6O_{24}](WO_{4(0.05)}ReO_{4(1.9)})$	7.94 ±0.10	6.02 ±0.08	6.00 ±0.17	39.7	1.904 ±0.03	0.048 ±0.01

Table 3.3: Refined powder X-ray data for mixed-anion sodalite.

Sample Type	Structural Formula	*a* (Å)	esd	χ^2
Re/Cl-SOD	$Na_8[Al_6Si_6O_{24}](Cl_{(2.1)}ReO_{4(0.003)})$	8.8885	±0.0002	2.76
Re/CO_3-SOD	$Na_8[Al_6Si_6O_{24}](CO_{3(1.0)}ReO_{4(0.02)})$	8.9691	±0.0002	8.07
Re/SO_4-SOD	$Na_{7.6}[Al_6Si_6O_{24}](SO_{4(0.96)}ReO_{4(0.08)})$	9.0785	±0.0004	3.60
Re/MnO_4-SOD	$Na_8[Al_6Si_{5.9}O_{24}](MnO_{4(1.1)} ReO_{4(0.97)})$	9.1258	±0.0005	1.32
Re/WO_4-SOD	$Na_{7.9}[Al_6Si_6O_{24}](WO_{4(0.05)}ReO_{4(1.9)})$	9.1527	±0.0002	6.05

a – unit cell parameter, esd – estimated standard deviation, and χ^2 – index of agreement.

Table 3.4: XANES spectral fitting results for mixed-anion sodalites.

Sample	ReO_2	p*	ReO_4-sodalite	p*
Re/Cl-SOD	0.18(6)†	0.017	0.82(5)	<0.001
Re/CO_3-SOD	0.08(5)	0.168	0.92(4)	<0.001
Re/SO_4-SOD	0.03(5)	0.545	0.97(4)	<0.001
Re/MnO_4-SOD	0.02(6)	0.828	0.98(5)	<0.001
Re/WO_4-SOD	0.00(2)	1.000	1.00(1)	<0.001

†The number in parentheses is the standard deviation in the same decimal place as the digit preceding it.

*p is the usual p-value.

Table 3.5: Ionic radii, hydration energy and ionic potential data for studied anions

Anions (X)	r (nm)	DIR (%)	Ionic Potential (Z/r)	Hydration Energies ($kJmol^{-1}$)
Cl^-	0.172[d]	51.2	0.58	-340[a]
CO_3^{2-}	0.189[c]	37.6	1.06	-1315[a]
SO_4^{2-}	0.230[a]	13.0	0.87	-1080[a]
NO_3^-	0.200[a]	30.0	0.50	-300 [a]
MnO_4^-	0.240[a]	8.3	0.42	-235[a]
WO_4^{2-}	0.267[b]	2.7	0.75	-702[e]
ReO_4^-	0.260[a]	0.0	0.39	-330[a]
TcO_4^-	0.252 [d]	3.2	0.40	-251 [d]

Where r represents the ionic radii of anions

[a] Thermodynamics of solvation of ions; Marcus et al. (1991)

[b] Ionic radius in aqueous solution; Marcus et al. (1988)

[c] Handbook of chemistry and physic; David et al. (2003)

[d] Physical factors in anion separation; Moyer et al. (1979)

[e] Hydration and extraction of oxyanion; Abramov et al. (2001)

DIR: Differences in ionic radii.

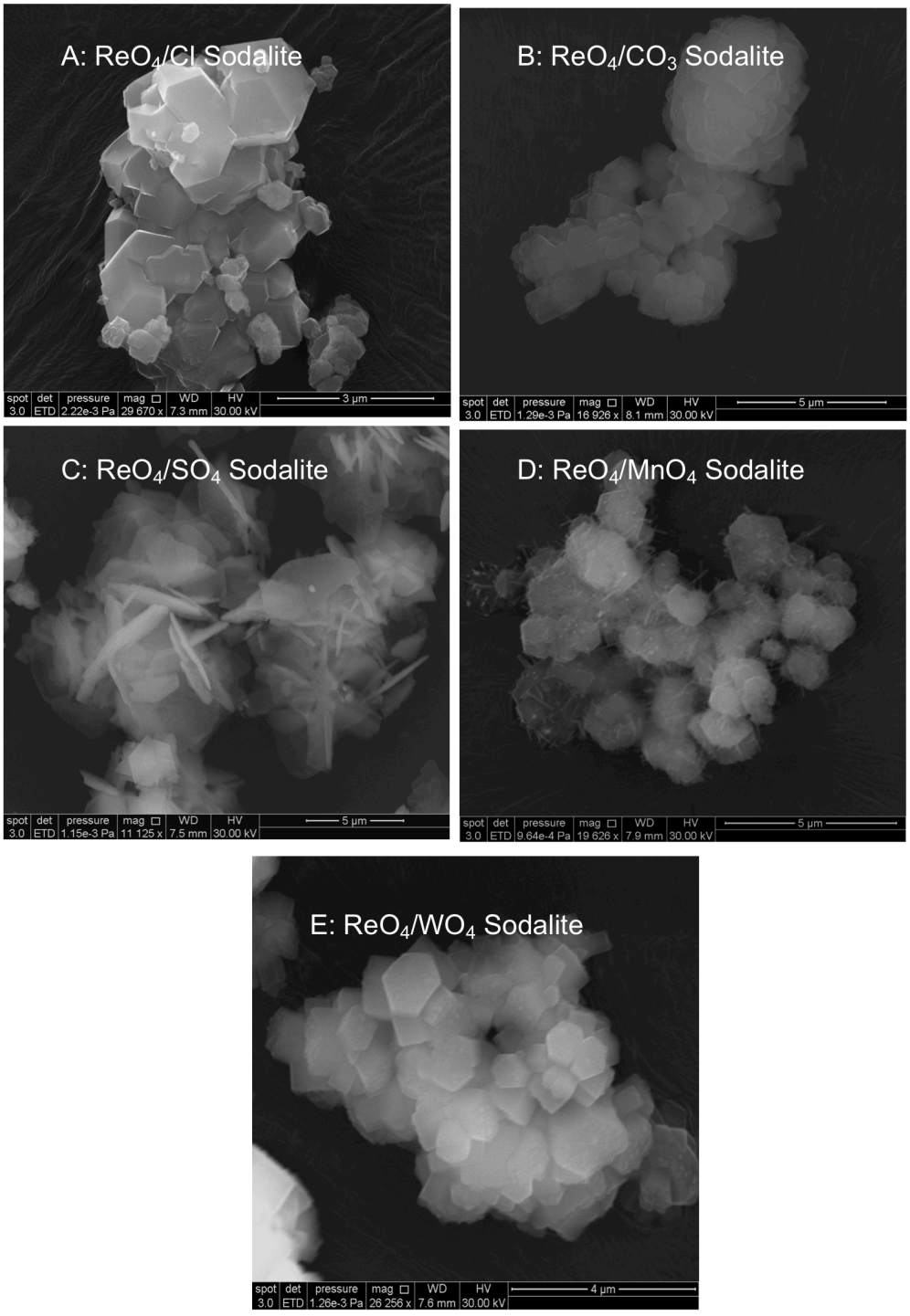

Figure 3.1: SEM images of mixed-anion sodalite formed in an equimolar ReO_4^-/ X^{n-} solution.

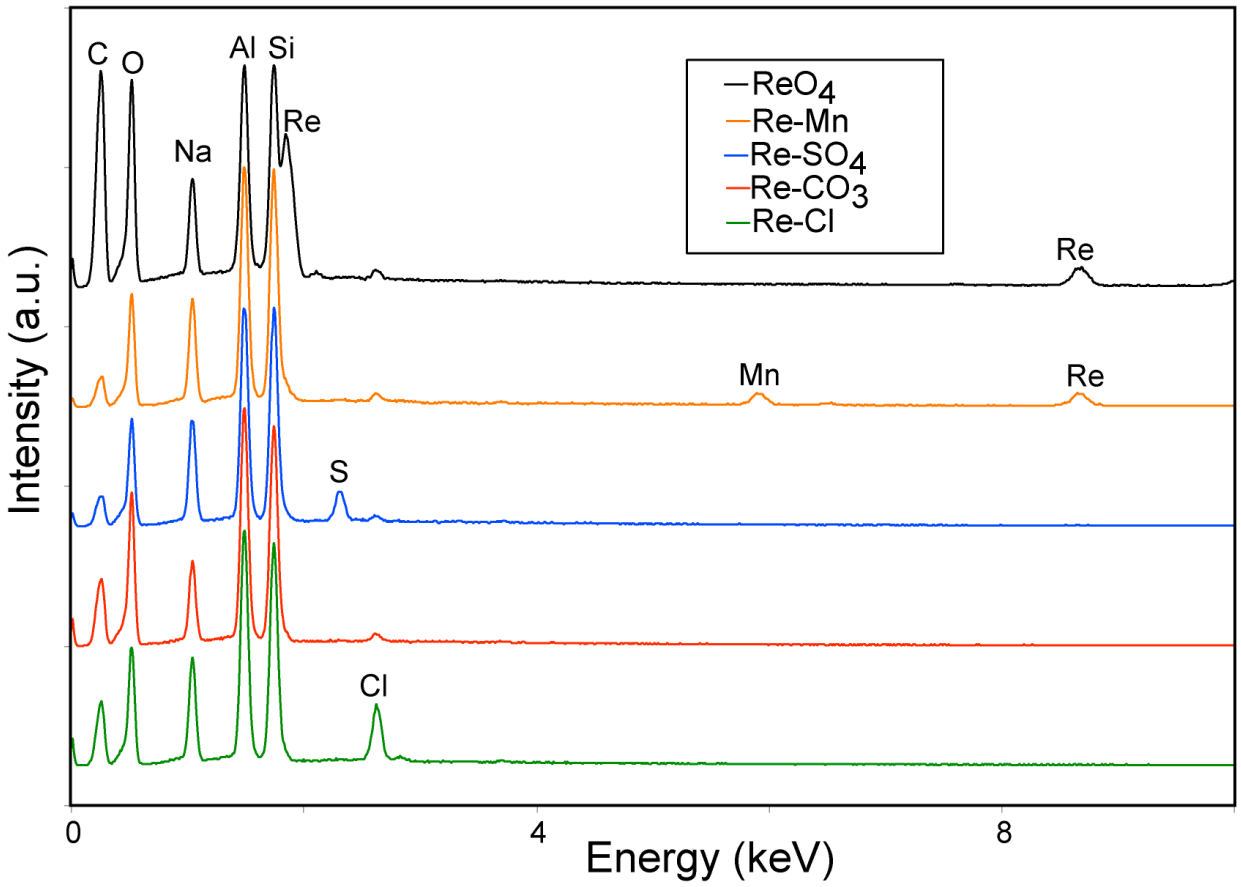

Figure 3.2: EDS spectra for mixed-anion sodalites: The additional Cl^- peaks in some of the samples are from the epoxy matrix used in preparing the samples for thin sections.

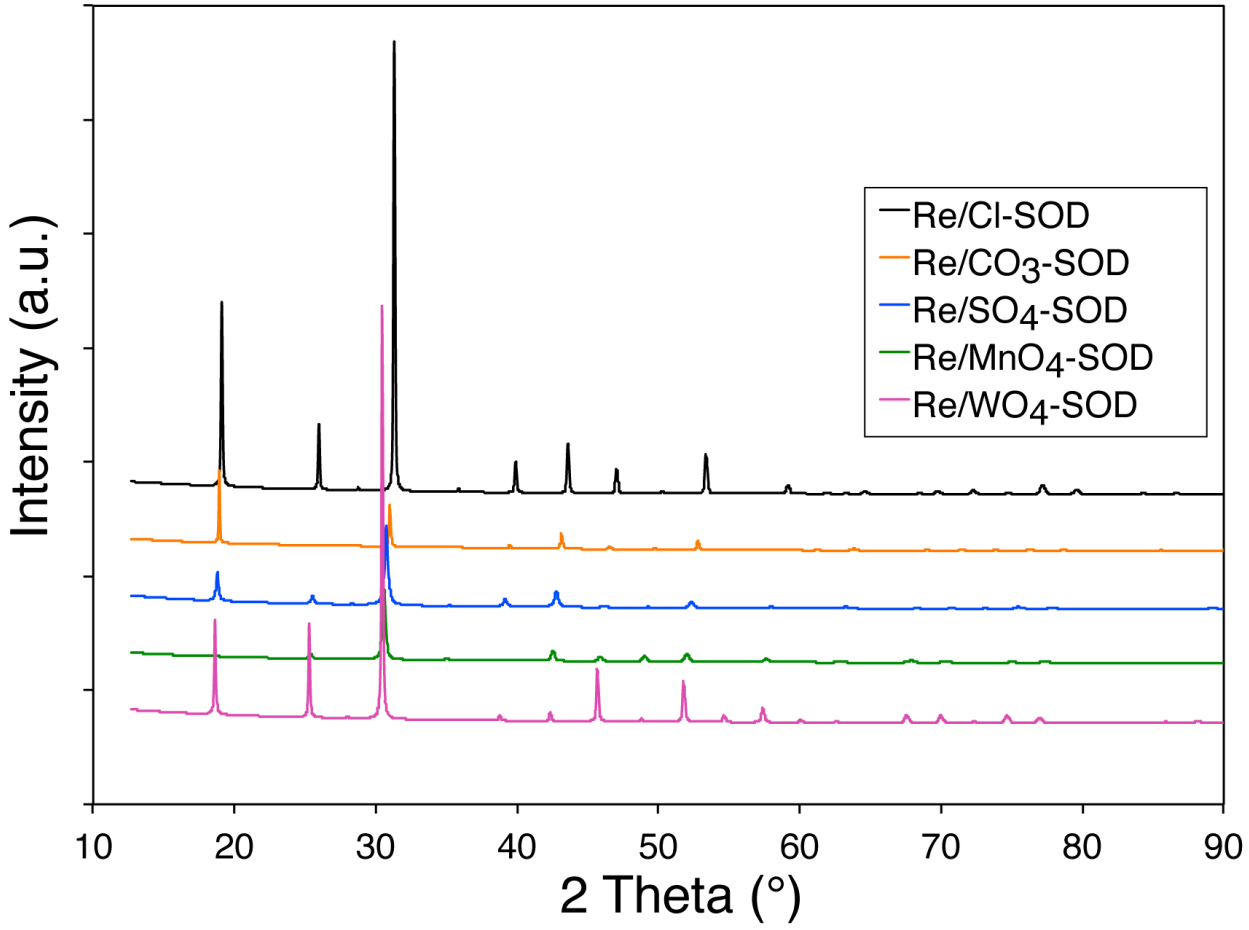

Figure 3.3: Refined powder X-ray spectra for mixed-anion sodalites.

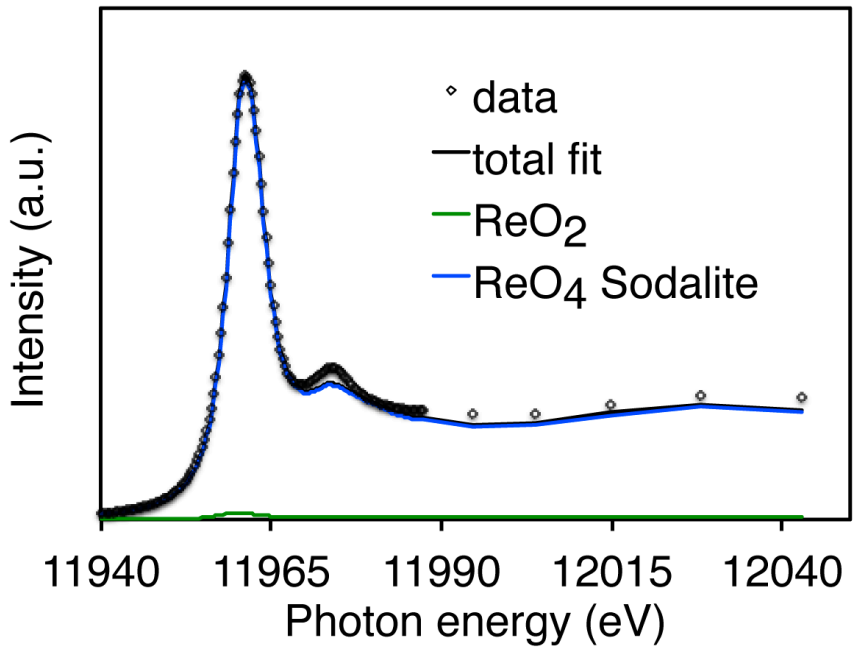

Figure 3.4: Rhenium L_2-XANES spectral data for ReO_4/MnO_4-sodalite; data are represented by dots, and the fit is shown by the black line. Results indicate Re(VII) oxidation state

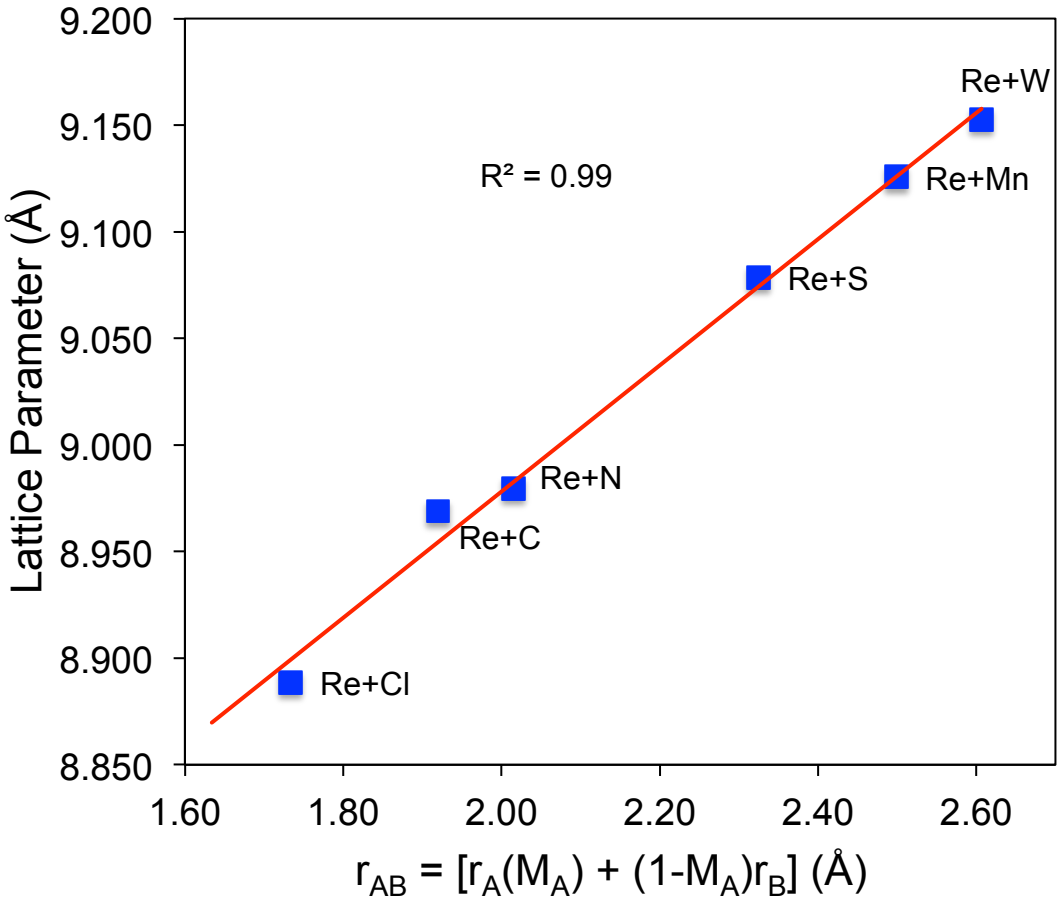

Figure 3.5: The dependence of lattice parameter on $r_{AB} = [r_A(M_A) + (M_{1-A})r_B]$. Data points are from Rietveld refinement of XRD data, and the red line is based on Vegard's Rule.

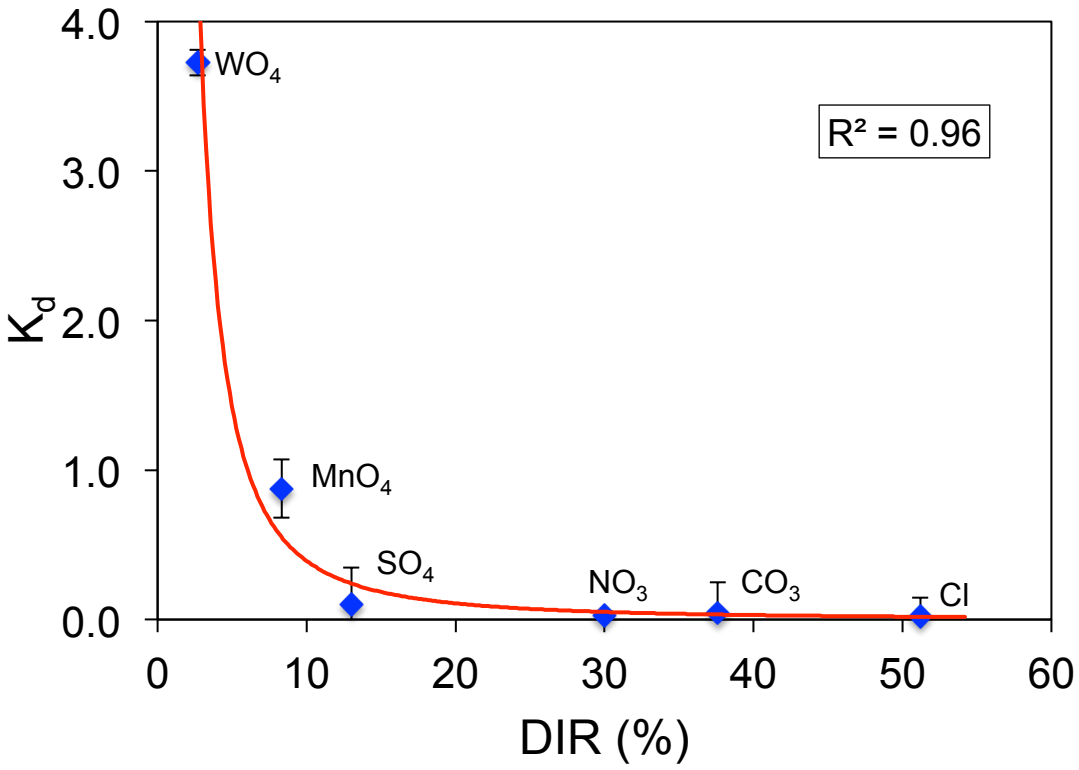

Figure 3.6: The distribution coefficient (K_d) graph for ReO_4^- sequestered in mixed-anion sodalite as a function of DIR; generally more than 90% of sodalite cages are filled with anions.

Chapter 4

Immobilization and Exchange of Perrhenate in Sodalite and Cancrinite

4.1 Abstract

Highly alkaline nuclear tank wastes containing key anionic contaminants have leaked into the subsurface at the U.S. Department of Energy Hanford Site. Laboratory studies showed that when simulated caustic tank wastes contact subsurface sediments, mineral dissolution and precipitation result in feldspathoid formation. Feldspathoids are environmentally important for waste management and disposal purposes because of their purported potential to sequester contaminants of interest ($^{99}TcO_4^-$ and $^{137}Cs^+$) into their frameworks.

We investigated the incorporation of perrhenate (ReO_4^-), a TcO_4^- surrogate, in the presence of competing anions (X) including OH^-, Cl^- on feldspathoid formation and under conditions mimicking tank solution compositions. The resulting solids were characterized by bulk products' chemical composition, structure and morphology.

This chapter will be submitted for publication to *Applied Geochemistry*: Dickson, J.O., Harsh, J.B., Flury, M., Pierce, E.M. (2014), Immobilization and Exchange of Perrhenate in Sodalite and Cancrinite (to be submitted)

Regardless of solution pH, sodalite formed in the presence of Cl^- and NO_2^- whereas nitrate (NO_3^-) promoted either cancrinite formation in 16 mol OH^-/kg or mixed sodalite/cancrinite in 1 mol OH^-/kg solutions. In the presence of Cl^-, NO_2^-, and NO_3^- less than 0.02 mole fraction of ReO_4^- was incorporated into the feldspathoid phase(s). The NO_2-sodalite and mixed NO_3-cancrinite/sodalite phases incorporated significantly more ReO_4^- than NO_3-cancrinite or Cl-sodalite phases but still only around 1% of the total sites. The ReO_4^- in ReO_4-sodalite, NO_2-sodalite, mixed NO_3-cancrinite/sodalite and NO_3-cancrinite was resistant to ion exchange with either NO_2^- or NO_3^-. The results imply that ReO_4^- does not compete well with smaller ions for incorporation into feldspathoids but, once sequestered, is difficult to exchange.

4.2 Introduction

At the U.S. Department of Energy's Hanford site in southeastern Washington, high-level radioactive wastes (HLW) containing an estimated 1900 kg of ^{99}Tc were has leaked into the vadose zone underneath the storage tanks (Crowley, 1997; Gephart and Lundgren, 1998). The highly variable waste is characterized as a highly alkaline (pH = ~10 to >14), high ionic strength solution (up to I = 18) with a density of 2.09 g/cm^3 and a temperature greater than 100°C (Pruess et al., 2002; Serne et al., 2001). The tank waste contains radionuclides of concern such as $^{137}Cs^+$, $^{90}Sr^+$, $^{99}TcO_4^-$, $^{125}I^-$, and chemical processing by-products (Na^+, $Al(OH)_4^-$, OH^-, NO_3^-, NO_2^- , CO_3^{2-}, Cl^-, SO_4^{2-}, PO_4^{3-}, Ni^+) and, aluminum and iron oxyhydroxides sludges (Kaplan and Serne, 1998; Qafoku et al., 2003a). Given the estimated inventory of ^{99}Tc in the waste – 19,730 curies (Ci), a long half life of 211,000 years and the high mobility due to weak adsorption to solid mineral phases as the pertechnetate oxyanion (TcO_4^-) under aerobic conditions, ^{99}Tc migration into the vadose zone water and groundwater poses long-term environmental risk hazard (Agnew et al., 1997; Zachara et al., 2007).

Previous investigations have shown that radionuclides, metals, and anions can be incorporated into feldspathoids (e.g., sodalite, cancrinite) that formed when tank leachate reacts with native Hanford sediments at elevated temperature and hyper-alkalinity (Chorover et al., 2008; Deng et al., 2006a; Deng et al., 2006b). Mattigod et al. (2002; 2006) indicated that perrhenate (ReO_4^-), a nonradioactive surrogate for $^{99}TcO_4^-$, can be incorporated into sodalite (Mattigod et al., 2006; Mattigod et al., 2002). Recent work by Pierce et al. (2014) suggests that ReO_4^- and SO_4^{2-} were simultaneously

incorporated into a mixed-anion sodalite. A mixed ReO_4/TcO_4-sodalite has been reportedly synthesized in the same laboratory (Pierce et al., 2014, submitted).

The open porous framework structure of cancrinite is made of layers of six-membered rings of SiO_4 and AlO_4 tetrahedra stacked along the hexagonal *c*-axis direction in an AB–AB sequence, resulting in the formation of the small ε-cages, and a large 12-ring channel along the *c*-axis. While the 6.0 Å-wide channels can accommodate water, large extra-framework cations and anions, the 2.5 Å ε-cages only house cations or water molecules, which can easily be substituted by other cations or small molecules in exchange experiments or during hydrothermal synthesis (Buhl et al., 2000). Sodalite consists of alternating SiO_4 and AlO_4 corner-sharing tetrahedra linked into four and six ring cages, which make up sodalite the β-cage. These cages are ~6.5 Å in diameter and are accessible through the 2.6 Å-wide six-membered rings that provide diffusion pathways for intra-framework ions (Depmeier, 2005). The β-cage is occupied by four cations tetrahedrally associated with an anion at the center of the cage. Because of the similarity in structural framework of the two feldspathoids, the characteristic XRD peaks used to distinguish cancrinite from sodalite are those of the 101 and 211 indices corresponding to d-spacings of ~4.67 and 3.24 Å respectively.

Although the effect of different anions on feldspathoid formation has been well studied (Barrer and Cole, 1970; Deng et al., 2006b), there exist lack of detailed information on anion selectivity in feldspathoids and the effect of this selectivity on ReO_4^- incorporation into feldspathoid phases. To our knowledge there are few systematic studies that address anion selectivity in feldspathoids, thus, the objective of our study is to (1) determine the role of solution composition (Cl^-, NO_2^-, and NO_3^-) on

formation of sodalite and cancrinite in the presence of ReO_4^- and the exchangeability of ReO_4^- from feldspathoids and, (2) elucidate the effect of alkalinity, aging time, and anion type on the solid phase formation and extent of ReO_4^- incorporation. We hypothesize that hyper-alkalinity and prolonged reaction time will strongly favor cancrinite formation over sodalite. We further hypothesize that upon contact with water solutions containing other competing anions, the sequestered ReO_4^- will not appreciably exchange from the porous framework in the short term.

4.3 Experimental Methods

4.3.1 Mineral Synthesis

Feldspathoids (sodalite and cancrinite) were synthesized in the laboratory according to the following procedures outlined by Deng et al. (2006a):

Cancrinite and sodalite were synthesized by mixing solutions of NaOH (1 mol/kg or 16 mol/kg), 0.5 *M* $NaAlO_2$, 0.175 *M* Na_2SiO_3, 0.5 *M* NaCl, 0.5 *M* $NaNO_2$ and 0.5 *M* $NaNO_3$ with varying concentrations of $NaReO_4$ (0.1 *M* or 0.5 *M*) in a 60-mL Teflon digestion bomb. The concentrations were based on concentrations reported for Hanford tank wastes and sediments (Deng et al., 2006b; Lichtner and Felmy, 2003; Qafoku et al., 2004). All chemical reagents were used as received. The bombs were capped, agitated and heated at 80 °C in an oven for 4 to 16 weeks. The mineral precipitates were washed three times with deionized water (0.054×10^{-3} dSm^{-1}) by centrifugation at 17,000 rcf. The solids were dried at 70^0C for 24 hours, weighed and subsamples dialyzed against deionized water until the electrolytic conductivity was ≤0.01 dSm^{-1}. The solids were digested in 3% nitric acid and the ReO_4^- contents were measured by

inductively coupled plasma mass spectrometry (Agilent 7700 ICP-MS, Santa Clara, CA). A summary of the synthesis condition is shown in Table 4.1.

4.3.2 Perrhenate exchange with NO_2^- and NO_3^-

Ion exchange experiments were conducted at room temperature (23 ±2°C) in a stirred batch system using the following feldspathoids: NO_2-sodalite, mixed NO_3-cancrinite/sodalite, NO_3-cancrinite, and ReO_4-sodalite and $NaNO_2$ or $NaNO_3$ aqueous solutions. The pure ReO_4-sodalite was synthesized from zeolite 4A using a method described by Liu and Navrotsky (2007). The particle size of the ReO_4-sodalite ranged from 0.34 to 9.35 μm. For the ion exchange experiments 0.05 g of the above-referenced feldspathoids were mixed with 10 mL of 0.1 *M* $NaNO_2$ or $NaNO_3$ in polypropylene bottles (liquid/solid ratio ~200:1). The bottles were shaken on a reciprocal shaker at ≈120 rpm for 96 hours. The suspensions were centrifuged at 17,000 rcf for 30 min. and filtered with 0.45 μm Acrodic Syringe filters. Rhenium concentration in the supernatant solutions was determined by ICP-MS.

4.4 Characterization of solid phases

4.4.1 Powder X-ray Diffraction Identification

X-ray diffraction (XRG-3100, Philips Analytical Inc., Mahwah, NJ) of dry powders was performed by scanning at 0.05° steps with a five second dwell time over 2 – 50° 2θ using Ni-filtered CuKα radiation (35 keV, 30mA, and λ = 1.54050 Å) and a graphite monochromator. Mineral identification was conducted by matching observed XRD peaks with published peaks for known minerals. Weight fractions of cancrinite and sodalite in the powder samples were determined from Rietveld refinements of

crystallographic data with GSAS with the EXPGUI interface (Toby, 2001) and reported structures of the following phases: $Na_8(AlSiO_4)_6(NO_2)_2$, $Na_8(AlSiO_4)_6(ReO_4)_2$, and $Na_6Ca_{1.5}(AlSiO_4)_6(CO_3)_{1.5}(H_2O)_{1.75}$ (Buhl et al., 1996; Hackbarth et al., 1999; Mattigod et al., 2006). During the Rietveld analysis the following crystallographic parameters were varied: the background (8 parameters), unit cell, Na position, Re/anion occupancy, peak shape (5 parameters: U, V, W, and two peak shape parameters), overall thermal parameter (B), and preferred orientation.

4.4.2 Electron Microscopy

Select samples were examined with a field emission scanning electron microscope (FESEM) with a field emission gun (FEI Quanta 200F, FEI Co., Hillsboro, OR) and Everhart-Thornley detector. The FESEM operates on an accelerating voltage of 30 keV with a resolution of 1 nm. Powder samples were mounted on carbon tabs and sputter-coated with platinum-palladium for analysis on the FESEM. Suspension drops of powder samples in deionized water were placed on a 200-mesh carbon-nickel stub, air-dried and photographs obtained on a high resolution, transmission electron microscopy (FEI Tecnai G^2, FEI Co., Hillsboro, OR) equipped with a LaB6 filament. Particle size measurements were determined by dynamic light scattering (DelsaNano C Particle Analyzer, Beckman Coulter Inc., Brea, CA) equipped with a 633 nm Helium-Neon laser.

4.5 Results

4.5.1 Structures

The XRD patterns are presented in Figure 4.1 and Table 4.2. Cancrinite was identified by the (101) and (211) Miller indices with corresponding *d*-spacings of ≈4.64 and 3.24

Å, respectively, while the (211) and (330) Miller indices corresponding to *d*-spacings of ≈3.64 and 2.10 Å were used for sodalite identification. The XRD analysis showed that in the presence of ReO_4^-/Cl^- and ReO_4^-/NO_2^- sodalite was the only dominant phase(s) formed in the 1 mol OH^-/kg and 16 mol OH^-/kg solutions. The unit cell parameters (*a*) of these sodalites ranged from 8.9473 to 8.9670 Å respectively. Cancrinite was the only mineral formed in the 16 mol OH^-/kg solutions containing equimolar ReO_4^-/NO_3^- ratio, while a mixed cancrinite/sodalite phase(s) (sodalite – 55-60%; cancrinite – 40-45 %) was observed in the 1 mol OH^-/kg solutions. The observed cancrinite lattice parameters: *a* and *c* range from 12.687 – 12.708 Å and 5.179 – 5.191 Å respectively. Aside from pure or mixed cancrinite and sodalite phase(s) no other minor phase(s) or inclusions were formed in the reacting solutions based on the observed XRD patterns.

4.5.2 Morphology

The SEM and TEM particles images are shown in Figures 4.2 and 4.3. The ReO_4/NO_3-cancrinite/sodalite formed in 1 mol OH^-/kg solution exhibited typical lepispheric morphology, while euhedral hexagonal morphology characterized ReO_4/NO_3-cancrinite formed in 16 mol OH^-/kg solutions. The ReO_4/NO_2-sodalite occurred as wedge-shaped blade particles in the 1 mol OH^-/kg solution whereas ReO_4/Cl-sodalites formed in the 16 mol OH^-/kg solutions were predominantly hexagonal crystallites. The feldspathoids morphologies were similar to those reported by Deng et al. (2006b) for similar phases. The particle size measurements presented in Figure. 4.4 and Table 4.3 suggest that the feldspathoid crystallite size increases with reaction time.

4.5.3 Rhenium Uptake

The ReO_4^- uptake data are presented in Table 4.4. The ReO_4^- sequestered by sodalite in the 1 mol OH^-/kg solution containing ReO_4^-/NO_2^- was ~1.5 – 10 times higher than that of the ReO_4/Cl- and ReO_4/NO_3-containing solutions. The concentration of ReO_4^- sequestered in the ReO_4/NO_2-sodalite ranges from 15.29 to 16.67 mmol/kg, which corresponds to 3.3 – 15.3% ReO_4^- uptake from the starting solutions (based on the initial ReO_4^- concentration of 0.1 – 0.5 *M*). The uptake of ReO_4^- by cancrinite from the 16 mol OH^-/kg solution corresponds to 0.75 – 2.81 mmol/kg (~0.6 – 0.8% of the solution ReO_4^-). The mixed cancrinite/sodalite phases contained roughly 2.3 – 6.7% of ReO_4^- relative to its concentration in solution. Feldspathoids formed in the equimolar ReO_4^-/X solution contained ~1.08 times higher ReO_4^- concentrations than those solutions with 0.2:1 ReO_4^-/X molar ratios. Feldspathoids aged for 16 weeks contained ~1.5 - 2.5 times more ReO_4^- than those aged for 4 and 8 weeks (Figure 4.5 and Table 4.4), however, this increase is not proportional to ReO_4^- concentration in solutions. Moreover ReO_4^- does not significantly increased in the feldspathoids even when solution ReO_4^- was increased five times.

4.5.4 Desorption Experiment

The result of the ion exchange experiment is presented in Table 4.5. After 96 hours of the ion exchange experiment the electrolyte containing NO_2^- desorbed approximately 0.24% of ReO_4^- from the NO_2-sodalite cages, while the NO_3^- solution exchanged roughly 0.36% of ReO_4^- from NO_3-cancrinite, ~0.29% from NO_3-cancrinite/sodalite and 0.22% from the ReO_4-sodalite. Moreover, with increase in particle size the resistance of the enclathrated ReO_4^- to ion exchange also increased

(Figure 4.4 and Table 4.3). These data demonstrate the resistance of the ReO_4^- sequestered in the feldspathoid framework to ion exchange with other competing anions.

4.6 Discussion

4.6.1 Effect of Alkalinity

Increasing OH^- concentration in the starting solutions resulted in the formation of feldspathoids with distinctly different morphologies and compositions. As OH^- concentration increases from 1 mol OH^-/kg to 16 mol OH^-/kg in the reacting solutions (simulants) containing ReO_4^-/X anions (X = NO_3^-, NO_2^- and Cl^-) the crystallinity and weight fractions of the cancrinite/sodalite phase(s) also increased (Table 4.4). In the presence of ReO_4^-/NO_3^- the 1 mol OH^-/kg solution contained 55 - 60 wt% of sodalite and 40 - 45 wt% of cancrinite, whereas in the presence of ReO_4^-/NO_2^- only sodalite formed (Table 4.4). The 16 mol OH^-/kg solution in the presence of ReO_4^-/NO_3^- was comprised entirely of cancrinite; when ReO_4^-/Cl^- was present only sodalite phases formed.

In agreement with Deng et al. (2006) the NO_3^- predominantly facilitated the formation of crystalline cancrinite phase(s) in highly alkaline solutions. Deng et al. (2006) reported that this preference is driven in part by the Si/Al molar ratio, whereby 1.4 – 35 ratios strongly favor the formation of crystalline cancrinite. Furthermore, varying the solution alkalinity resulted in the formation of three morphological variations of feldspathoids: Lepispheric/needle-shaped, wedge-shaped blade, and euhedral particles. Lepispheric/needle-shaped sodalite and cancrinite predominantly formed in 1 mol OH^-/kg solution containing ReO_4^-/NO_3^- (Figures 4.2A and 4.3A) whereas in the

presence of ReO_4^-/NO_2^- wedge-shaped sodalite occurred (Figures 4.2C and 4.3C). Euhedral hexagonal crystallites characterized the sodalite and cancrinite formed in the 16 mol OH^-/kg solution containing either ReO_4^-/Cl^- or ReO_4^-/NO_3^- (Figures 4.2B, D and 4.3B, D).

4.6.2 Feldspathoid Formation in the Presence of Different Anions

The identity of anions present in the 0.35 Si/Al molar ratio solutions significantly affects the formation pathway of feldspathoids. When ReO_4^- and NO_3^- anions were added concomitantly to the 1 mol OH^-/kg solution, a mixed cancrinite/sodalite was the dominant phase(s) (Figures 4.2A and 4.3A), whereas the 16 mol OH^-/kg solution promoted the formation of pure cancrinite phase(s) (Figures 4.2B and 4.3B). On the other hand, NO_2^- and Cl^- in the presence of ReO_4^- favored predominantly the formation of pure sodalite phase(s) regardless of the solution alkalinity (Figures 4.2C-D and 4.3C-D). This implies that anions such as NO_2^- and Cl^- serve as suitable templates for sodalite formation irrespective of solution alkalinity. Deng et al. (2006b) reported similar findings in their study, where Cl^- and NO_2^- favored the formation of sodalite over cancrinite, while NO_3^-, CO_3^{2-}, and SO_4^{2-} promoted cancrinite formation (Deng et al., 2006b).

4.6.3 Feldspathoid Formation with Time

The type of feldspathoids formed was strongly influenced by the combined effects of solution alkalinity and the aging time. Increasing the solution alkalinity from 1 mol OH^-/kg to 16 mol OH^-/kg and reaction time from 4 to 8 weeks in the presence of NO_3^- and ReO_4^-, the products varied from a mixed sodalite/cancrinite phase(s) to predominantly pure cancrinite (Figures 4.2A-B and 4.3A-B). In the 16 mol OH^-/kg

solution aged for four weeks in the presence of NO_3^- and ReO_4^- only cancrinite was formed in solution (Figure 4.2B and Table 4.4); however, reducing the alkalinity to 1 mol OH^-/kg coupled with an increased reaction time to 8 weeks resulted in the formation of mixed sodalite/cancrinite in which sodalite slightly dominates over cancrinite (Figure 4.2A and Table 4.4). This implies that cancrinite is the stable phases in concentrated NaOH solution containing NO_3^- and ReO_4^-.

The size of the feldspathoids crystallites increases with aging time. The wedge-shaped NO_2-sodalite crystallites observed in the 1 mol OH^-/kg samples were generally larger than the lepispheric cancrinite/sodalite particles, and the euhedral cancrinite crystallites formed in the 16 mol OH^-/kg samples (Figure. 4.4 and Table 4.3).

4.6.4 Effect of ReO_4^- concentration on feldspathoid formation

As ReO_4^-/NO_3^- molar ratios were varied from 0.2 to 1 in the 1 mol OH^-/kg and 16 mol OH^-/kg solutions the amounts of ReO_4^- immobilized in the feldspathoids slightly increased. The equimolar ReO_4^-/NO_3^- solutions sequestered ReO_4^- at ~1.7 times greater than the solutions containing 0.2 ReO_4^-/NO_3^- molar ratio. Similar trends were observed for the ReO_4^-/NO_2^- sodalite, where the equimolar ReO_4^-/NO_2^- solution incorporated ReO_4^- at ~1.08 times higher than the 0.2 ReO_4^-/NO_2^- ratio solution. The cancrinite phase(s) formed in the equimolar ReO_4^-/NO_3^- solution sequestered ~3.8 times more ReO_4^- than the 0.2 ReO_4^-/NO_3^- molar ratio solution (Figure 4.6 and Table 4.4).

In general the ReO_4/NO_2-sodalite sequestered ReO_4^- at 1.5 – 2.5 times higher concentration than any of the other mixed-anion feldspathoids. Furthermore, in the presence of NO_3^- the cancrinite/sodalite phase(s) formed in the 1 mol OH^-/kg solution

immobilized an estimated 4 – 9 times more ReO_4^- than cancrinite formed in the 16 mol OH^-/kg solution, suggesting the more open channels of cancrinite frameworks relative to that of sodalite (Figure 4.6 and Table 4.4).

4.6.5 Stability of ReO_4^- to Ion Exchange

Upon contact with either NO_2^- or NO_3^- electrolyte solutions at 23 ±2°C, the relative amounts of ReO_4^- desorbed from the studied feldspathoid phases (ReO_4-sodalite, NO_2-sodalite, mixed NO_3-cancrinite/sodalite and NO_3-cancrinite) in the ion exchange experiment ranged from 0.22% to 0.36% respectively (Table 4.5). The NO_3-cancrinite released the most amount of ReO_4^-, while the ReO_4-sodalite the least amount.

In general, the studied feldspathoids released much smaller amounts of ReO_4^- over the duration of the experiments in support of our hypothesis that the NO_2^- or NO_3^- anions would not significantly displace ReO_4^- from the feldspathoid cages. The resistance of the enclathrated ReO_4^- in the feldspathoids to ion exchange was likely due to the high activation energy required for desorption through the feldspathoid channel/apertures. This is supported by the work of Mon et al. (2005) who reported that the release of Cs^+ from sodalite increased slightly as temperature was increased from 23°C to 50°C due to high activation energy required for the exchange process.

4.6.6 Anion Template Effects on Feldspathoid Formation

The nature of the ions partly determines which type of feldspathoid is formed – sodalite or cancrinite. Nitrite and Cl^- favor the nucleation of sodalite, while NO_3^- depending on solution compositions (pH, Al/Si ratio and competing anions) may foster either sodalite or cancrinite nucleation. Deng et al. (2006b) reported that the structure-directing NO_3^- and SO_4^{2-} anions strongly promote the nucleation of cancrinite and sodalite. Similar

anion template effects were reported by Barrer (1981) and Bosnar et al. (2004) in their studies where Cl^-, Br^-, I^-, ClO_4^- and HCO_2^- favored sodalite formation, while SO_4^{2-}, NO_3^-, CrO_4^- and MnO_4^- induced cancrinite formation.

The template effect is attributed to the ion size and charge balance restrictions imposed by the feldspathoid topology on the extra-framework anions (Deng et al., 2006b). Although the charge imbalance on the sodalite framework requires a monovalent anion to compensate the cation-cation repulsion, divalent or trivalent anions would be less stable in the cage due to more cations required for charge neutrality or incomplete site occupancy by the anions. This may explain why CO_3^{2-} and SO_4^{2-} tend to favor the formation of the open channels of cancrinite.

Sodalite cages can host guest anions of varying size due to cooperative tilting and deformation of its frameworks. It has been shown that feldspathoid cage size and composition are strongly influenced by ion size, type and selectivity (Dickson et al., 2014, submitted). For example, in the absence of other competing anions the lattice parameter of NO_3-sodalite formed with a 2.0-Å NO_3^- is 8.9762 Å while that of ReO_4-sodalite containing a 2.6-Å ReO_4^- is 9.1535 Å. In the presence of more than one anion, sodalite shows a preference for the smaller ion, suggesting that the smaller cages are more stable (Figure 4.7). In cancrinite, on the other hand, ReO_4^- incorporation is negligible. Although in Figure 4.7, a small amount of ReO_4^- is incorporated into the cancrinite and mixed sodalite-cancrinite phases, however, the amount is too small to ascertain if it was associated with cancrinite.

4.7 Conclusions and Implications

We synthesized ReO_4/X-bearing feldspathoids (cancrinite, sodalite and mixed

cancrinite/sodalite). Alkalinity, solution compositions, anion size and extra-framework species selectivity determined the feldspathoid type and composition. Nitrite and Cl^- facilitated sodalite formation (Figures. 4.2, 4.3 and Table 4.4) while NO_3^- in 16 mol OH^-/kg solutions favored cancrinite, and mixed cancrinite/sodalite formation in the 1 mol OH^-/kg solution. Only the solid phases containing sodalite incorporated significant amount of ReO_4^-. The ReO_4^- in the solid phases was not easily exchanged with NO_2^- or NO_3^-.

Because ReO_4^- is a suitable surrogate for $^{99}TcO_4^-$, our results suggest that sodalite can sequester ^{99}Tc as TcO_4^-, but smaller competing anions will be preferred. We used a closed system for our experiment, however, in an open system such as a waste stream or subsurface condition below leaking tanks, other mineral phases such as zeolite, nosean, nepheline may form that have a higher preference for larger anions. For example, Pierce et al. (2014) showed that NO_3^- will incorporate into cancrinite and SO_4^{2-} into nosean; whereas Cl^-, NO_2^- and ReO_4^- will be intercalated into sodalite. Thus, TcO_4^- could sequester into the sodalite after other competing anions have been selectively removed by earlier-forming phases.

4.8 Tables and Figures

This page is intentionally left blank

Table 4.1: Summarized conditions for the hydrothermal syntheses.

Sample ID	NaOH (M)	X† (M)	$NaReO_4$ (M)	Aging Time (wks)
Re:NO_3-C+S-1	1	0.5	0.1	8
Re:NO_3-C+S-2	1	0.5	0.5	8
Re:NO_3-C-1	16	0.5	0.1	4
Re:NO_3-C-2	16	0.5	0.5	4
Re:NO_2-S-1	1	0.5	0.1	16
Re:NO_2-S-2	1	0.5	0.5	16
Re:Cl-S-1	16	0.5	0.1	4

†X represents the different anions: NO_3^-, NO_2^-, and Cl^-. C = cancrinite, S = sodalite.

Table 4.2: Unit cell and refinement parameters for mixed-anion feldspathoid

Samples ID	Sodalite	Cancrinite		χ^2
	a (Å)	a (Å)	c (Å)	
Re:NO_3-C+S-1	8.9748(4)	12.687(2)	5.179(1)	3.47
Re:NO_3-C+S-2	8.9890(1)	12.708(4)	5.196(3)	6.74
Re:NO_3-C-1		12.691(1)	5.188(1)	7.62
Re:NO_3-C-2		12.698(2)	5.191(1)	10.42
Re:NO_2-S-1	8.9480(3)			9.56
Re:NO_2-S-2	8.9670(7)			3.23
Re:Cl-S-1	8.9373(4)			3.29

a – unit cell parameter, esd – estimated standard deviation, χ^2 – weighted agreement factors.

Table 4.3: Particle size data (mean volume distribution) for select mixed-anion Feldspathoid.

Percentile	Re:NO_3-C-2 Size (μm)	Re:NO_3-C+S-2 Size (μm)	Re:NO_2-S-2 Size (μm)
10	0.441	0.130	0.313
25	0.651	0.253	0.568
40	0.964	0.490	1.029
50	1.254	0.762	1.532
60	1.63	1.19	2.28
75	2.86	2.31	4.14
85	3.82	3.59	6.16
95	5.11	5.57	9.17

Table 4.4: Feldspathoid weight fraction and ReO_4^-/anion concentrations.

	Feldspathoid (wt%)			
Sample ID	Sodalite	Cancrinite	X (mmol/kg)	ReO_4 in solid (mmol/kg)
Re:NO_3-C+S-1	55	45	1632.24 ± 2.30	3.68 ± 0.05
Re:NO_3-C+S-2	60	40	1695.43 ± 26.13	6.91 ± 0.13
Re:NO_3-C-1		100	1630.64 ± 10.46	0.75 ± 0.02
Re:NO_3-C-2		100	1550.18 ± 30.37	2.81 ± 0.16
Re:NO_2-S-1	100		1646.90 ± 12.77	15.39 ± 0.07
Re:NO_2-S-2	100		1674.23 ± 27.37	16.67 ± 0.15
Re:Cl-S-1	100		1745.15 ± 6.95	1.62 ± 0.03

Table 4.5: Solution ReO_4^- after aqueous exchange of feldspathoids with NO_2^- or NO_3^- for 4 days.

Feldspathoid type	ReO_4^- in feldspathoids (mmol/kg)	Solution ReO_4^- following 4 days of suspension (mmol/kg)		(%)
Re:NO_3-C-2	2.81 ±0.16	ReO_4^-/NO_3^-	0.01	0.36
Re:NO_3-C+S-2	6.91 ±0.13	ReO_4^-/NO_3^-	0.02	0.29
Re:NO_2-S-2	16.67 ±0.15	ReO_4^-/NO_2^-	0.04	0.24
ReO_4-sodalite	1388.80 ± 17.72	ReO_4^-/NO_3^-	3.05 ±0.03	0.22

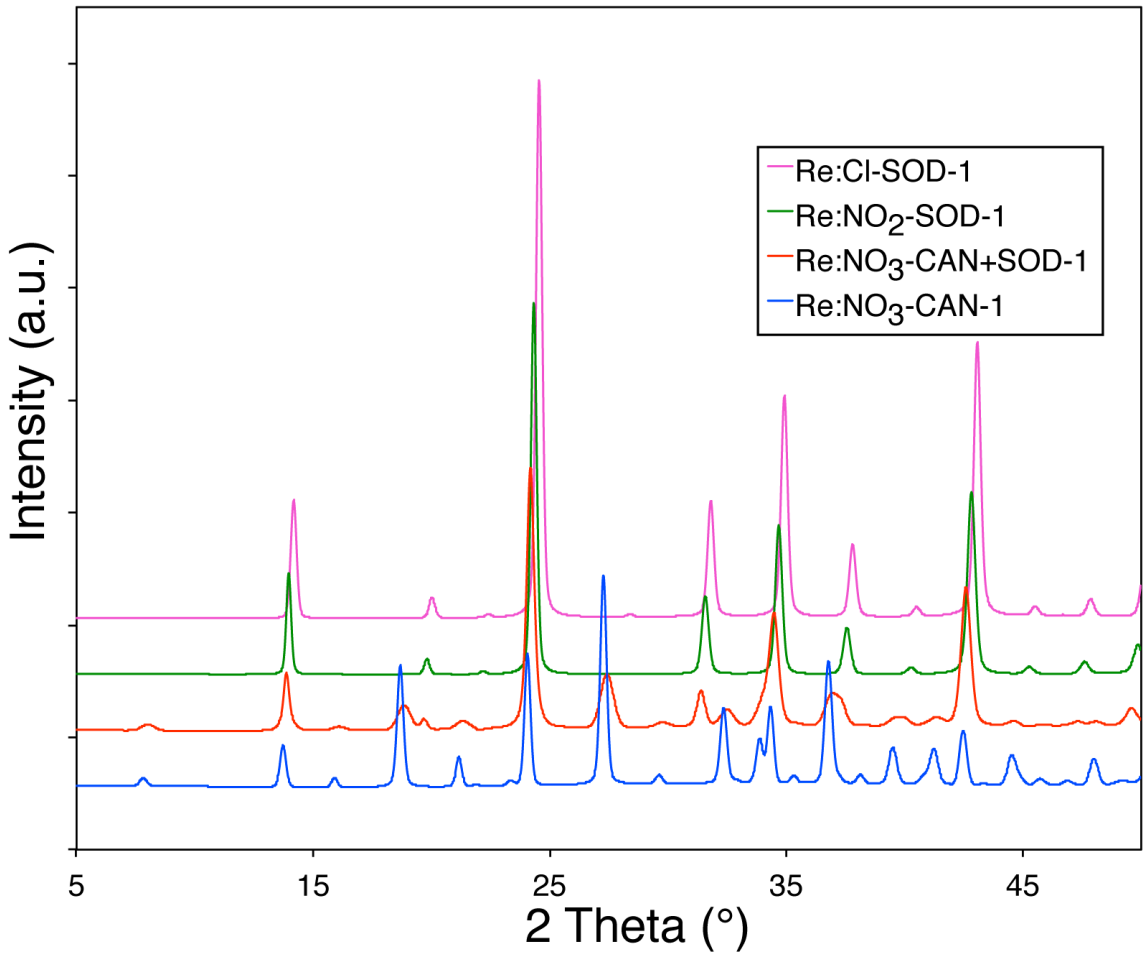

Figure 4:1: Refined powder X-ray spectra for mixed-anion feldspathoids, Re:X-SOD-1 contains 0.2 ReO_4^-/X^- solution ratio, X are anions (Cl^-, NO_2^-, and NO_3^-).

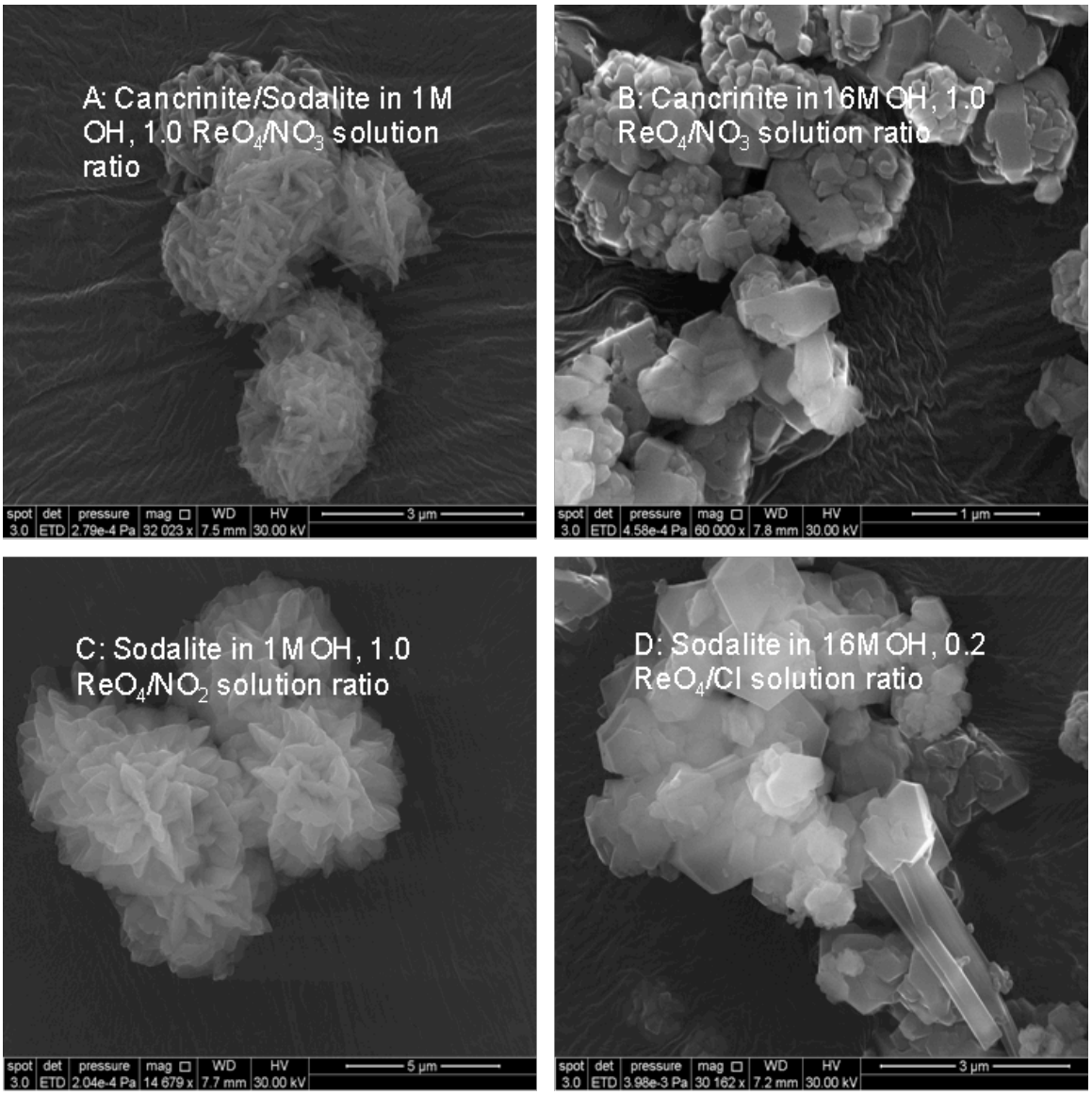

Figure 4.2: SEM images of ReO_4/X-feldspathoids formed in either 1 mol OH^-/kg or 16 mol OH^-/kg solutions containing 0.2 – 1.0 ReO_4^-/X ratios.

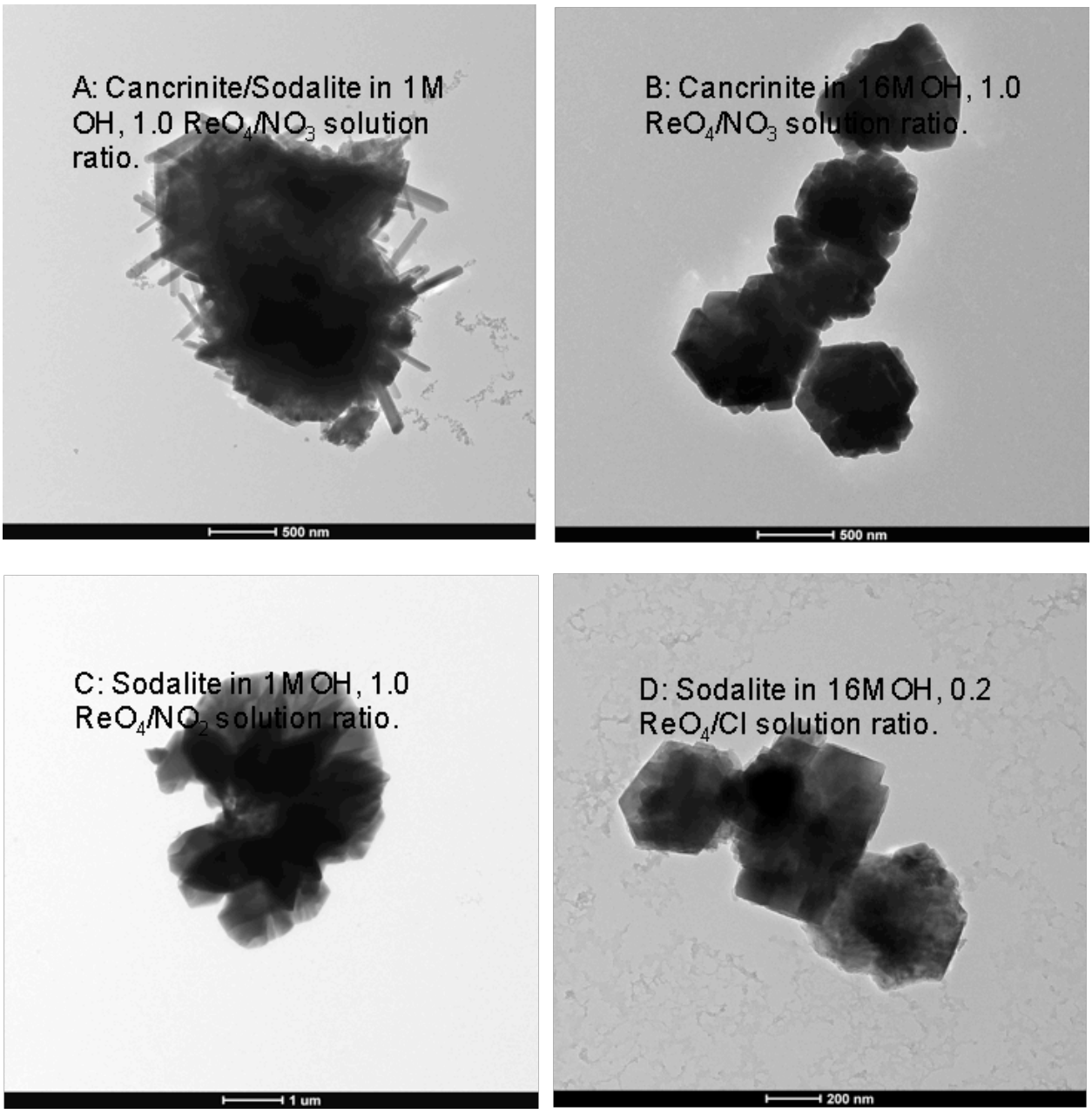

Figure 4.3: TEM images of mixed-anion feldspathoids formed in either 1 mol OH^-/kg or 16 mol OH^-/kg solutions containing 0.2 – 1.0 ReO_4^-/X ratios.

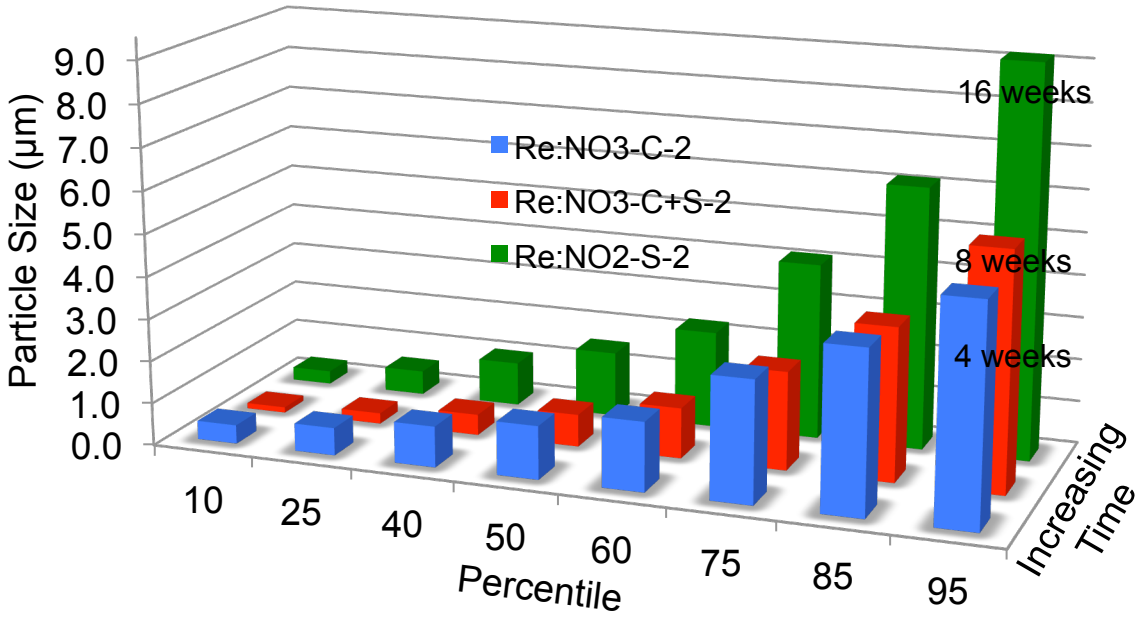

Figure 4.4: Mixed-anion feldspathoid particles formed in either 1 mol OH^-/kg or 16 mol OH^-/kg solutions containing 0.2 – 1.0 ReO_4^-/X ratios.

In product labels: C = Cancrinite; S = Sodalite; Blue square = 4 weeks; Red square = 8 weeks and Green square = 16 weeks

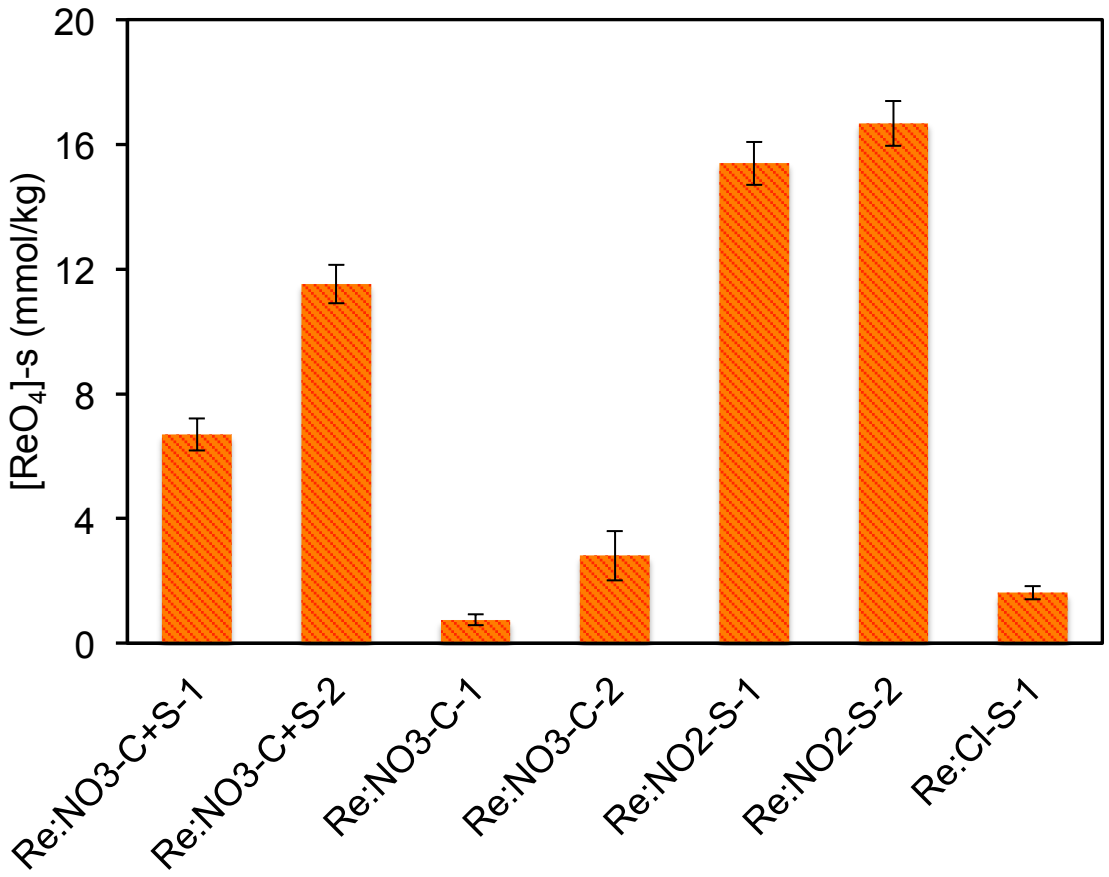

Figure 4.5: ReO_4^- incorporated into mixed-anion feldspathoids.

In product labels, C = cancrinite, S = sodalite, "1" designate either 1 mol OH^-/kg or 16 mol OH^-/kg solutions containing 0.2 – 1.0 ReO_4^-/X ratio and "2" designates a 1.0 ReO_4^-/X ratio, where X = Cl^-, NO_2^- or NO_3^-

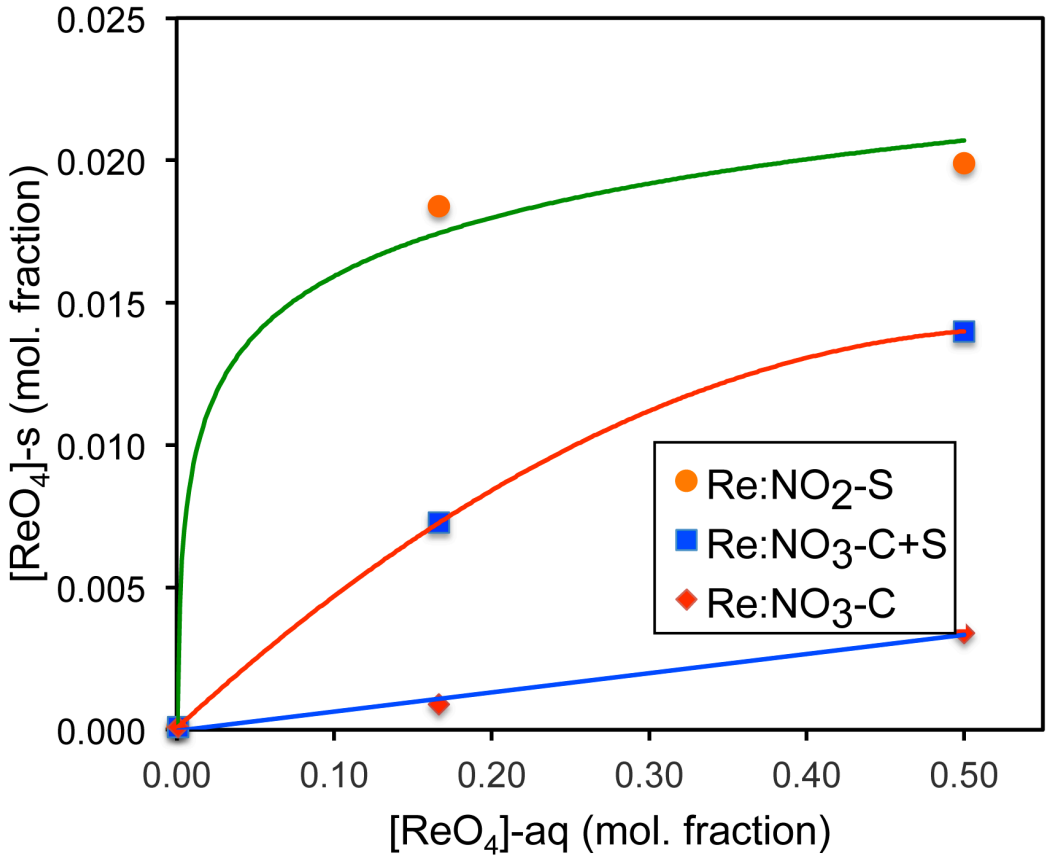

Figure 4.6: Variation of ReO_4^- sequestered in mixed-anion feldspathoids with ReO_4^-/X solution ratios.

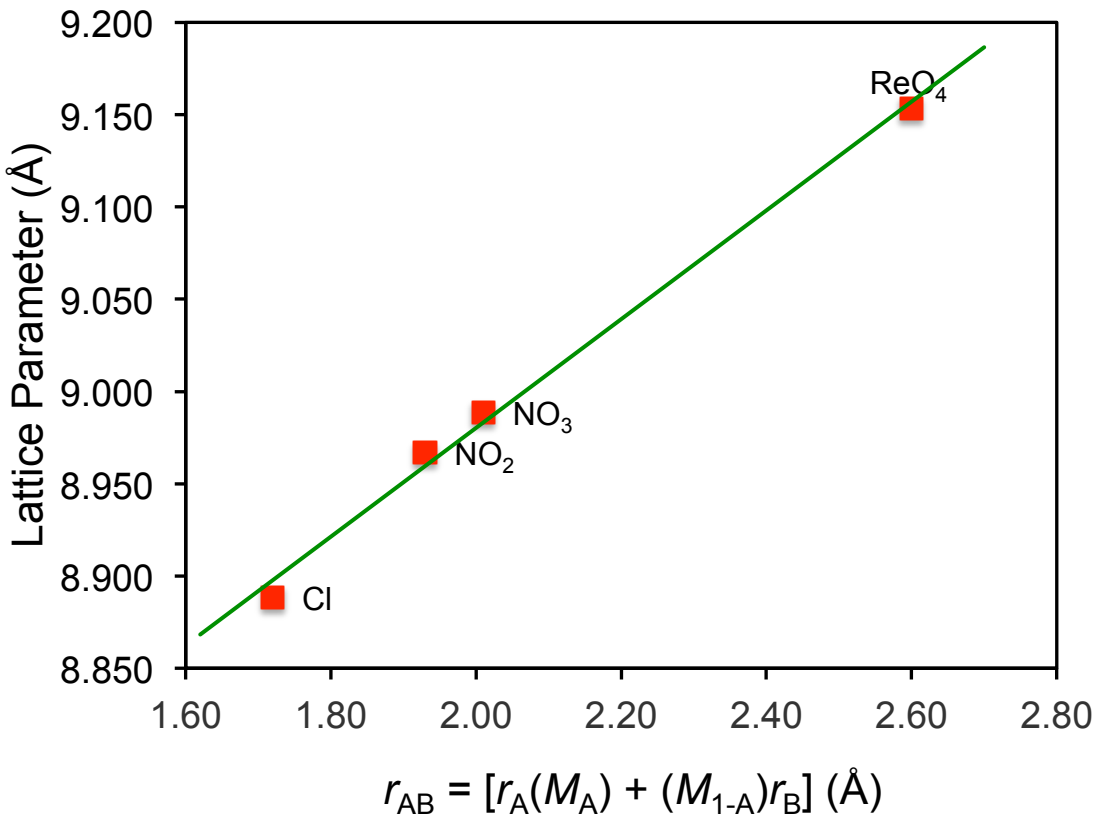

Figure 4.7: The Graph showing the dependence of lattice parameter on $r_{AB} = [r_A(M_A) + (M_{1-A})r_B]$. Data points are from Rietveld refinements of XRD data, and the green line is based on Vegard's Rule.

Chapter 5

Summary and Conclusions

The application of versatile porous framework materials (cancrinite, sodalite, zeolite, MOF) as a selective medium for sequestration of long-lived anionic radionuclides (e.g., $^{99}TcO_4^-$, $^{129}I^-$, $^{75}SeO_4^{2-}$) represents a key component in closing the back end of the nuclear fuel cycle. Furthermore, advanced knowledge of factors governing anion selectivity in feldspathoids is critical for their potential application in anion-sequestration processes.

The overarching objective of this dissertation was to better understand the effect of competing anions of varying size and charge (Cl^-, CO_3^{2-}, NO_3^-, SO_4^{2-}, MnO_4^-, and WO_4^{2-}) on incorporation of perrhenate into sodalite formed under alkaline conditions of Hanford tank waste streams, subsurface and engineered wastes, vitrification products, and materials formed by chemical weathering. Here, we used batch studies to synthesize mixed-anion sodalites from solutions mimicking waste tank solution compositions. Using binary solutions containing ReO_4^- and a competing anion X (Cl^-, CO_3^{2-}, NO_3^-, SO_4^{2-}, MnO_4^-, or WO_4^{2-}), we studied (1) the competitive incorporation of perrhenate (ReO_4^-), a chemical surrogate for $^{99}TcO_4^-$, into mixed perrhenate/nitrate (ReO_4^-/NO_3^-) sodalite, (2) anion selectivity in mixed-anion sodalite, and (3) exchangeability of ReO_4^- from feldspathoids.

The main conclusions of this dissertation are as follows:

1. The synthesis of mixed ReO_4/NO_3-sodalite over a range of ReO_4^-/NO_3^- in solution strongly favors the formation of the NO_3-sodalite phases

2. The sodalite β-cages preferred NO_3^- anion an estimated 30 ±2 times more than ReO_4^-
3. Smaller anions are more competitive than ReO_4^- for the mixed sodalite β-cages
4. Similarity in ionic radius (DIR of ≤15%), and charge (ionic potential) promote the competitive incorporation of ReO_4^- into the mixed-anion sodalite
5. The mixed sodalite selectivity for ReO_4^- in the presence of competing anions increases in the order as follows: $Cl^-<CO_3^{2-}<NO_3^-<SO_4^{2-}<<MnO_4^-<WO_4^{2-}$
6. Nitrite and chloride anions predominantly facilitated sodalite formation, whereas NO_3^- in 16 mol OH^-/kg solutions favored cancrinite nucleation, and mixed cancrinite/sodalite in 1 mol OH^-/kg solutions.
7. The ReO_4^- sequestered in the feldspathoid was not easily exchanged with NO_2^- or NO_3^-

Although recent results suggest that feldspathoids can immobilize ^{99}Tc in the presence of other anions contained in the waste streams assuming similarity in ionic radii, our findings indicate that ReO_4^-, a surrogate for TcO_4^-, was significantly intercalated into mixed sodalite only when competing anions are present in very low concentrations or completely absent. Our experiment used a closed system, however, in an open system such as a waste stream or subsurface condition below leaking tanks, other mineral phases such as zeolite, nosean, nepheline may form that have a higher preference for larger anions. Thus, TcO_4^- could sequester into sodalite after other competing anions have been selectively removed by earlier-forming phases. Moreover, partial substitution of Si with Al in the framework may results in the formation of mixed aluminate sodalite possessing higher affinity for TcO_4^-. These suggestions need to be

explored further through a series of batch and leaching experiments. Further work is needed in open systems, with a greater range of conditions, and at realistic ^{99}Tc concentrations to mimic waste-impacted subsurface sediments and managed waste streams to determine if mixed-anion sodalites may be relevant sequestering phase(s).

Bibliography

Acar, A. C., Yucel, H., and Culfaz, A.: The synthesis and sodium-silver ion exchange of sodalites, Chem. Eng. Commun., 190, 861-882, 2003.

Agnew, S. F., Boyer, J., R.A, C., Duran, T. B., FitzPatrick, J. R., Jurgensen, K. A., Ortiz, T. P., and Young, B. L.: Hanford chemical and radionuclide inventories: HDW Model, Los Alamos National Laboratory: Los Alamos, NMLA-UR-96-3860, 1997.

Barrer, R. M.: Zeolites and Their Synthesis, Zeolites, 1, 130-140, 1981.

Barrer, R. M. and Cole, J. F.: Chemistry of soil minerals. Part VI. Salt entrainment by sodalite and cancrinite during their synthesis, Journal of the Chemical Society A: Inorganic, Physical, Theoretical, doi: 10.1039/j19700001516, 1970. 1516, 1970.

Barrer, R. M. and Vaughan, D. E. W.: Trapping of inert gases in sodalite and cancrinite crystals, J. Phys. Chem. Solids, 32, 731-743, 1971.

Bibler, N. E. and Jurgensen, A. R.: Leaching Tc-99 from SRP glass in simulated tuff and salt groundwaters, 1988, 585-593.

Bloom, P. R., Weaver, R. M., and McBride, M. B.: The spectrophotometric and fluorometric determination of aluminum with 8 hydroxy quinoline and butyl acetate extraction Soil Science Society of America Journal, 42, 713-716, 1978.

Bosnar, S., Antonic-Jelic, T., Bronic, J., Krznaric, I., and Subotic, B.: Influence of anions on the kinetics of zeolite A crystallization: a population balance analysis, J. Cryst. Growth, 267, 270-282, 2004.

Brenchley, M. E. and Weller, M. T.: Synthesis and structures of $M_8[AlSiO_4]_6(XO_4)_2$, M=Na, Li, K, X=Cl, Mn Sodalites, Zeolites, 14, 682-686, 1994.

Buhl, J. C. and Lons, J.: Synthesis and crystal structure of nitrate enclathrated sodalite $Na_8(AlSiO_4)_6(NO_3)_2$, J. Alloys Compd., 235, 41-47, 1996.

Buhl, J. C., Reich, D., Mundus, C., and MullerWarmuth, W.: Si-29 MAS NMR investigations on the crystallization of nitrite-sodalite, React. Kinet. Catal. Lett., 58, 13-18, 1996.

Buhl, J. C., Stief, F., Fechtelkord, M., Gesing, T. M., Taphorn, U., and Taake, C.: Synthesis, X-ray diffraction and MAS NMR characteristics of nitrate cancrinite $Na_{7.6}$ $[AlSiO_4]_6(NO_3)_{1.6}(H_2O)_2$, J. Alloys Compd., 305, 93-102, 2000.

Choi, S., Chorover, J., Bowers, G., Strepka, C., Mueller, K. T., Rivera, N. A., and O'Day, P. A.: GEOC 124-Characterization of Sr and Cs sequestration and mineral transformation from reaction of Hanford sediments and caustic waste, Abstracts of Papers of the American Chemical Society, 232, 2006.

Chorover, J., Choi, S., Rotenberg, P., Serne, R. J., Rivera, N., Strepka, C., Thompson, A., Mueller, K. T., and O'Day, P. A.: Silicon control of strontium and cesium

partitioning in hydroxide-weathered sediments, Geochim. Cosmochim. Acta, 72, 2024-2047, 2008.

Crowley, K. D.: Nuclear waste disposal: The technical challenges (vol 50, pg 32, 1997), Physics Today, 50, 85-85, 1997.

Custelcean, R. and Moyer, B. A.: Anion separation with metal-organic frameworks, Eur. J. Inorg. Chem., doi: 10.1002/ejic.200700018, 2007. 1321-1340, 2007.

Deng, Y. J., Flury, M., Harsh, J. B., Felmy, A. R., and Qafoku, O.: Cancrinite and sodalite formation in the presence of cesium, potassium, magnesium, calcium and strontium in Hanford tank waste simulants, Appl. Geochem., 21, 2049-2063, 2006a.

Deng, Y. J., Harsh, J. B., Flury, M., Young, J. S., and Boyle, J. S.: Mineral formation during simulated leaks of Hanford waste tanks, Appl. Geochem., 21, 1392-1409, 2006b.

Depmeier, W.: The sodalite family - A simple but versatile framework structure. In: Micro- and Mesoporous Mineral Phases, Ferraris, G. and Merlino, S. (Eds.), Reviews in Mineralogy & Geochemistry, 2005.

Dickson, J. O., Harsh, J. B., Flury, M., Lukens, W. W., and Pierce, E. M.: Competitive incorporation of perrhenate and nitrate into sodalite, Environ. Sci. Technol., 2014, submitted. 2014, submitted.

Ewing, R. C.: Nuclear waste forms for actinides, Proceedings of the National Academy of Sciences of the United States of America, 96, 3432-3439, 1999.

Fazal, T.: High temperature studies of sodalites, 2011.A Thesis for the MRes in Materials Chemistry and Nanochemistry, Department of Chemistry, University of Birmingham, 116 pp., 2011.

Frising, T. and Leflaive, P.: Extraframework cation distributions in X and Y faujasite zeolites: A review, Microporous Mesoporous Mater., 114, 27-63, 2008.

Gee, G. W., Oostrom, M., Freshley, M. D., Rockhold, M. L., and Zachara, J. M.: Hanford site vadose zone studies: An overview, Vadose Zone Journal, 6, 899-905, 2007.

Gephart, R. E. and Lundgren, R. E.: A Guide to understanding the Technical Issues, 1998.

Gephart, R. E. and Lundgren, R. E.: Hanford Tank Cleanup: A Guide to understanding the Technical Issues, Pacific Northwest National Laboratory, Richland, Washington, 1995.

Golcar, G. R., Colton, N. G., Darab, J. G., and Smith, H. D.: Hanford tank waste simulants specification and their applicability for the retrieval, pretreatment, and vitrification processes, Pacific Northwest National Laboratory, Richland, WashingtonBNFL-RPT-012, 2000.

Grundy, H. D. and Hassan, I.: The crystal structure of a carbonate-rich cancrinite, Can. Mineral., 20, 239-251, 1982.

Hackbarth, K., Gesing, T. M., Fechtelkord, M., Stief, F., and Buhl, J. C.: Synthesis and crystal structure of carbonate cancrinite $Na_8(AlSiO_4)_6CO_3 3.4H_2O$, grown under low-temperature hydrothermal conditions, Microporous Mesoporous Mater., 30, 347-358, 1999.

Icenhower, J. P., Qafoku, N. P., Zachara, J. M., and Martin, W. J.: The biogeochemistry of Technetium: A review of the behavior of an artificial element in the natural environment, American Journal of Science, 310, 721-752, 2010.

Inagaki, Y., Idemitsu, K., Arima, T., Maeda, T., Ogawa, H., and Itonaga, F.: Alteration-phase formation and associated cesium release during alteration of R7T7 waste glass, in: 2001 MRS Fall Meeting, Boston, MA2002, 2002.

Johnson, G. M., Mead, P. J., and Weller, M. T.: Structural trends in the sodalite family, PCCP, 1, 3709-3714, 1999.

Kaplan, D. I. and Serne, R. J.: Pertechnetate exclusion from sediments, Radiochimica Acta, 81, 117-124, 1998.

Lichtner, P. C. and Felmy, A. R.: Estimation of Hanford SX tank waste compositions from historically derived inventories, Computers & Geosciences, 29, 371-383, 2003.

Liu, Q. and Navrotsky, A.: Synthesis of nitrate sodalite: An in situ scanning calorimetric study, Geochim. Cosmochim. Acta, 71, 2072-2078, 2007.

Liu, Q., Xu, H., and Navrotsky, A.: Nitrate cancrinite: Synthesis, characterization, and determination of the enthalpy of formation, Microporous Mesoporous Mater., 87, 146-152, 2005.

Lukens, W. W., McKeown, D. A., Buechele, A. C., Muller, I. S., Shuh, D. K., and Pegg, I. L.: Dissimilar behavior of technetium and rhenium in borosilicate waste glass as determined by X-ray absorption spectroscopy, Chem. Mater., 19, 559-566, 2007.

Marcus, Y.: Thermodynamics of solvation of ions. Part 5 - Gibbs free energy of hydration at 298.15-K Journal of the Chemical Society-Faraday Transactions, 87, 2995-2999, 1991.

Mashal, K., Harsh, J. B., Flury, M., Felmy, A. R., and Zhao, H. T.: Colloid formation in Hanford sediments reacted with simulated tank waste, Environ. Sci. Technol., 38, 5750-5756, 2004.

Mattigod, S. V., McGrail, B. P., McCread, D. E., Wang, L. Q., Parker, K. E., and Young, J. S.: Synthesis and structure of perrhenate sodalite, Microporous Mesoporous Mater., 91, 139-144, 2006.

Mattigod, S. V., Serne, J., McGrail, B. P., and LeGore, V. L.: Radionuclide Incorporation in Secondary Crystalline Minerals from Chemical Weathering of Waste Glasses. MRS Proceedings, 713, JJ5.1 in: 2001 MRS Fall Meeting, Boston, MA2002, 2002.

Missimer, D. M. and Rutherford, R. L.: Preparation and initial characterization of fluidized bed steam reforming pure-phase standards, Savannah River National Laboratory, Aiken, SC, Technical report for DOE EM-31 DE-AC09-08SR22470, 2013.

Mon, J., Deng, Y. J., Flury, M., and Harsh, J. B.: Cesium incorporation and diffusion in cancrinite, sodalite, zeolite, and allophane, Microporous Mesoporous Mater., 86, 277-286, 2005.

Moyer, B. A. and Bonnesen, P. V.: Physical Factors in Anion Separation. In supramolecular chemistry of anions. Bianchi, A., Bowman-James, K., and Garcia-Espana, E. (Eds.), Wiley-VCH, New York, 1979a.

Moyer, B. A. and Bonnesen, P. V. (Eds.): Physical Factors in Anion Separation. Supramolecular chemistry of anions, Wiley-VCH, New York, 1979b.

Pearce, C. I., Liu, J., Baer, D. R., Qafoku, O., Heald, S. M., Arenholz, E., Grosz, A. E., McKinley, J. P., Resch, C. T., Bowden, M. E., Engelhard, M. H., and Rosso, K. M.: Characterization of natural titanomagnetites ($Fe_{3-x}Ti_xO_4$) for studying heterogeneous electron transfer to Tc(VII) in the Hanford subsurface, Geochim. Cosmochim. Acta, 128, 114-127, 2014.

Peretyazhko, T. S., Zachara, J. M., Kukkadapu, R. K., Heald, S. M., Kutnyakov, I. V., Resch, C. T., Arey, B. W., Wang, C. M., Kovarik, L., Phillips, J. L., and Moore, D. A.: Pertechnetate (TcO_4^-) reduction by reactive ferrous iron forms in naturally

anoxic, redox transition zone sediments from the Hanford Site, USA, Geochim. Cosmochim. Acta, 92, 48-66, 2012.

Pierce, E. M., Lilova, K., Lukens, W. W., Navrotsky, A., Fritts, J., Rawn, C., Jantzen, C. M., Missimer, D. M., and Huq, A.: Structure and thermochemistry of perrhenate sodalite and perrhenate/pertechnetate guest-guest sodalite, Proceeding of the national Academy of Science, 2014, submitted.

Pierce, E. M., Lukens, W. W., Fitts, J. P., Jantzen, C. M., and Tang, G.: Experimental determination of the speciation, partitioning, and release of perrhenate as a chemical surrogate for pertechnetate from a sodalite-bearing multiphase ceramic waste form, Appl. Geochem., 42, 47-59, 2014.

Pruess, K., Yabusaki, S., Steefel, C., and Lichtner, P.: Fluid Flow, Heat Transfer, and Solute Transport at Nuclear Waste Storage Tanks in the Hanford Vadose Zone, Vadose Zone Journal, 1, 68-88, 2002.

Qafoku, N. P., Ainsworth, C. C., Szecsody, J. E., Bish, D. L., Young, J. S., McCready, D. E., and Qafoku, O. S.: Aluminum effect on dissolution and precipitation under hyperalkaline conditions: II. Solid phase transformations, Journal of Environmental Quality, 32, 2364-2372, 2003a.

Qafoku, N. P., Ainsworth, C. C., Szecsody, J. E., and Qafoku, O. S.: Aluminum effect on dissolution and precipitation under hyperalkaline conditions: I. Liquid phase transformations, Journal of Environmental Quality, 32, 2354-2363, 2003b.

Qafoku, N. P., Ainsworth, C. C., Szecsody, J. E., and Qafoku, O. S.: Transport-controlled kinetics of dissolution and precipitation in the sediments under alkaline and saline conditions, Geochim. Cosmochim. Acta, 68, 2981-2995, 2004.

Ravel, B. and Newville, M.: Athena, Artemis, Hephaestus: Data analysis for X-ray absorption spectroscopy using Ifeffit, Journal of Synchrotron Radiation, 12, 537-541, 2005.

Serne, R. J., Bjornstad, B. N., Keller, J. M., Thorne, P. D., Lanigan, D. C., Christensen, J. N., and Thomas, G. S.: Conceptual models for migration of key groundwater contaminants through the vadose zone and Into the unconfined aquifer below the B-complex, Pacific Northwest National Laboratory, Richland, WashingtonPNNL-19277, 496 pp., 2010.

Serne, R. J., Lindenmeier, C. W., and Schaef, H. T.: Geochemical conditions in the vadose zone at leaking single-shell tanks in the B-BX-BY waste management area in Hanford's 200 E area, Abstracts of Papers of the American Chemical Society, 222, U492-U492, 2001.

Stein, A., Ozin, G. A., and Stucky, G. D.: Class-B sodalites - nonstoichiometric silver, sodium halosodalites, JACS, 114, 8119-8129, 1992.

Taylor, D. and Henderson, C. M. B.: A computer model for the cubic sodalite structure, Phys. Chem. Miner., 2, 325-336, 1978.

Toby, B. H.: EXPGUI, a graphical user interface for GSAS, J. Appl. Crystallogr., 34, 210-213, 2001.

Trill, H.: Sodalite solid solution systems: Synthesis, topotactic transformations, and Investigation of framework-guest and guest-guest interactions, PhD Dissertation, Universität Münster, 187 pp., 2002.

Trill, H., Eckert, H., and Srdanov, V. I.: Mixed halide sodalite solid solution systems. Hydrothermal synthesis and structural characterization by solid state NMR, J. Phys. Chem. B, 107, 8779-8788, 2003.

Trill, H., Eckert, H., and Srdanov, V. I.: Topotactic transformations of sodalite cages: synthesis and NMR study of mixed salt-free and salt-bearing sodalites, J. Am. Chem. Soc., 124, 8361-8370, 2002.

USDOE.: Vadose zone characterization project at the Hanford tank farms: AX tank farm report, Pacific Northwest National Laboratory, Richland, Washington, 1997.

Weaver, R. M., Syers, J. K., and Jackson, L. M.: Determination of silica in citrate-bicarbonate-dithionite extracts of soils, Soil Science Society of America Journal, 32, 497-501, 1968.

Weber, W. J., Navrotsky, A., Stefanovsky, S., Vance, E. R., and Vernaz, E.: Materials Science of High-Level Nuclear Waste Immobilization, MRS Bull., 34, 46-53, 2009.

Weller, M. T. and Wong, G.: Mixed halide sodalites, Eur. J. Solid State Inorg. Chem., 26, 619-633, 1989.

Weller, M. T., Wong, G., Adamson, C. L., Dodd, S. M., and Roe, J. J. B.: Intracage reactions in sodalites, Journal of the Chemical Society-Dalton Transactions, doi: 10.1039/dt9900000593, 1990. 593-597, 1990.

Zachara, J. M., Serne, J., Freshley, M., Mann, F., Anderson, F., Wood, M., Jones, T., and Myers, D.: Geochemical processes controlling migration of tank wastes in Hanford's vadose zone, Vadose Zone Journal, 6, 985-1003, 2007.